Spring 1-31-2019

DEVELOPMENT OF WIRELESS PEBBLE FOR PACKED BED HEAT TRANSFER MEASUREMENTS AND MACHINE LEARNING-AIDED ACCIDENT DIAGNOSIS FOR LOSS OF FLOW ACCIDENT (LOFA)

Dongjune Chang
University of New Mexico

Follow this and additional works at: https://digitalrepository.unm.edu/ne_etds

Part of the Nuclear Engineering Commons

Dongjune Chang

Candidate

Nuclear Engineering

Department

This thesis is approved, and it is acceptable in quality and form for publication:

Approved by the Thesis Committee:

Prof. Youho Lee, Chairperson

Prof. Cassiano R. E. de Oliveira

Prof. Sang Lee

i

DEVELOPMENT OF WIRELESS PEBBLE FOR PACKED BED HEAT TRANSFER MEASUREMENTS AND MACHINE LEARNING-AIDED ACCIDENT DIAGNOSIS FOR LOSS OF FLOW ACCIDENT (LOFA)

by

DONGJUNE CHANG

B.S., Mechanical Engineering & Mathematical Science, KAIST, Daejeon, 2010
M.S., Mechanical Engineering, KAIST, Daejeon, 2012

THESIS

Submitted in Partial Fulfillment of the
Requirements for the Degree of

Master of Science

Nuclear Engineering

The University of New Mexico
Albuquerque, New Mexico

May 2019

ACKNOWLEDGMENT

I wish to acknowledge the **University of New Mexico's Nuclear Engineering Department** for funding this research and providing the means by which I was able to complete my education at UNM. I would also like to acknowledge my research and academic advisor and the chair of the thesis committee, Dr. Youho Lee, Assistant Professor of Nuclear Engineering, because we were able to start two new kinds of studies that did not exist in the nuclear field. Many thanks are due to other members of the committee, including Dr. Sang Lee, Assistant Professor of Department of Mechanical Engineering, and Dr. Cassiano R. E. de Oliveira, Assistant Professor of Department of Mechanical Engineering for their helpful suggestions and valuable feedback and comments.

I appreciate the help I received from two lab research assistant professors, Dr. Maolong Liu and Dr. Amir Ali, and from Dr. Seong Gu Kim and my graduate student colleagues, Soon Lee, David Weitzel, and Mingfu He, who are working on related topics.

Special thanks are due to the members of my family, especially my wife Seoyeong Kim. Dad, mom and sister Suhyeon who helped me when I was in economic difficulties and confusion were also very grateful. I could not have achieved this without their patience, support, understanding, and hope for better things to come.

Development of Wireless Pebble for Packed Bed Heat Transfer Measurements and Machine Learning-Aided Accident Diagnosis for Loss of Flow Accident (LOFA)

by

Dongjune Chang

B.S., Mechanical Engineering & Mathematical Science, KAIST, 2010,

M.S., Mechanical Engineering, KAIST, 2012,

M.S., Nuclear Engineering, University of New Mexico, 2019

ABSTRACT

In the first study, a novel wireless pebble for scale experiments is developed, and a simple heat transfer experiment is conducted to determine the difference in the local heat transfer coefficient. Based on the fact that the use of Dowtherm A between approximately 57–87 °C is an alternative to the normal use of the FliBe temperature range of 600–700°C, a new-concept wireless device in a scaled experiment is introduced. This device consists of a 63.5 mm diameter metal shell and contains a built-in customized circuit board and battery for driving temperature measurements and wireless data transfer. The circuit board used for receiving temperature measurements from several type K thermocouples is based on the ATmega328 microprocessor (MCU). This board collects temperature at multiple points and send data to the receiver wirelessly. Also, the results from the experiment on the wireless communication between multiple devices are presented. The single wireless pebble did not change the value of the averaged heat transfer coefficient, even when the airflow rate changed and the attachment structure of Thermocouple (TC) was changed. Because the averaged heat transfer coefficient did not change significantly in the

orientation of the internal heater, it could easily expand into several wireless pebbles. Lastly, the demonstration of three multiple wireless pebbles indicates that our suggested wireless pebbles can greatly help to estimate the local heat transfer coefficient. The results of the validation process will be extended to multiple wireless pebbles in future packed pebble-beds. This research is applicable to a case study for scaled experiments with packed pebble-beds for fluoride salt-cooled high-temperature reactors. We expect that this study will provide an experimental basis for pebbles for those who wish to use a non-invasive wireless device, which offer a powerful approach to investigating heat transfer coefficients in a non-invasive manner and to designing randomly packed configurations for further studies.

In the second study, a prediction of accident diagnosis using machine learning was performed. The simple case of an unprotected loss of flow accident (LOFA) was selected for simulation for a fuel pin at the start of different flow rates. The obtained outlet temperatures were used to identify the relationship between peak fuel temperatures and flow rate changes using a support vector machine (SVM). The SVM, trained with the core outlet temperature, provided an accurate prediction ($R^2 > 0.9$) for changes in mass flow rate and peak surface temperature cladding in the early phase of LOFA transience (~0.5 s), unless the amount of training data was limited.

This illustrates that the key accident features are reflected well in the reactor core's early response (i.e., core outlet temperature). This implies two possibilities. The first is to implement a different diagnostic framework from the current behavioral response to a prolonged progression of the accident. The second is to provide effective guidance for accident mitigation strategies in the early stages of accident progression.

v

The high predictability (i.e., $R^2 > 0.9$) presented in the early phase of unprotected LOFA shows that the core outlet temperature is strongly correlated with both the change in flow rate and the peak surface cladding temperature throughout the entire transience. This strong correlation between different physical parameters allows for the possibility of interdependent detector systems by reducing the traditional boundaries of physical location and physical quantities in accident response and progress detection.

Table of Contents

List of Figures

xiii

xiv

List of Tables

1. Introduction

This paper presents two in-depth studies on two independent topics in nuclear engineering. The first study introduces a new methodology to measure local heat transfer coefficients using wireless devices in a scaled heat transfer experiment, and the other one is a diagnostic study of a simple nuclear accident case using machine learning. These two different topics have a common purpose in the safety analysis of nuclear reactors, but they are intended for different nuclear applications, which are molten-salt reactors and pressurized water reactors (PWRs), respectively. In this section, the author will briefly introduce what motivates each research initiative and what the relevant research is.

1.1 Wireless pebble research

The key technical challenge in chemical and nuclear engineering [1], [4], [6]–[11] has been the efficient and extensive correlation equations of heat transfer coefficients in pebble-bed systems. The Nusselt number correlations of individual heat transfer models have been shown in many experimental studies [8], [10]–[13] to predict the heat transfer in packed beds. Subsequent to the particle-liquid heat transfer approach in Wakao and Kaguei [10], considerable effort and experimental work was carried out, showing changes in experimental correlation based on several related parameters, such as the Prandtl number, the Reynolds number, and bed porosity. Until recently, most of the literature, which has usually studied chemical and catalytic applications, was primarily concerned with predicting the pebble-bed core temperature distribution. Also, these studies usually rely on calculating the overall heat transfer of all pebbles, rather than finding the value of the heat transfer coefficient of an individual pebble.

1

However, unlike chemical applications, nuclear engineering requires safety standards that can eliminate potential safety risks. Recent studies [14]–[16] have reported that there is a measurable difference between the surface temperatures of packed bed systems, suggesting that the statistical heat transfer distribution due to the random placement of pebbles should be considered. Thus, different heat transfer problems, such as local hot spots due to "random packaging," have been carefully considered in the nuclear engineering field. In addition, the measurement or calculation of overall values does not ensure that all the different heat transfer coefficients at all locations are free from problems.

Fluoride salt-cooled high temperature reactors (FHR) are one of the applications experiencing this problem. Many studies related to packed pebble-beds for FHRs have widely conducted owing to the reactor's passive safety features under atmospheric pressure, pool type configuration, and higher thermal efficiency compared to conventional nuclear systems. However, its performance and safety rely heavily on the hydraulic thermal information at its core, such as different local flow profiles, and heat transfers around spherical fuels due to random packing density. The local heat transfer effect of this scheme should be carefully investigated to meet the challenge of finding an adequate model for fluid flow, heat transfer, and structural analysis.

Many research projects have started to define the problems that occur locally by increasing the number of thermocouples (TCs) around the heat test sections. Nazari [14] and Huddar [15] reported well-defined and successful experiments. Another group [16] used heat flux sensors in order to evaluate heat generation. Even though they have considered problems related to random packing, there are several limitations. First, the TCs used in those studies were invasive TCs that interacted with the coolant fluid. Also, due to

2

the limited number of TCs, it was difficult to cover the local hot spots, and this leads to a loss of statistical information for randomly packed pebbles. In this case, there may be significant uncertainty with regard to reactor core temperature predictions.

The first study suggests a new device that measures temperatures at multiple points wirelessly and enables us to estimate local heat transfer coefficients in randomly packed pebbles. The usage of a wireless module, unlike the conventional method of using wires, aids the measurement of temperatures in a non-invasive fashion. This approach leads improves on invasive temperature-measurement methods and overcomes the limited number of TCs along the test sections. For this reason, this approach is quite different from that of previous experimental studies. Furthermore, the wireless device can be used to determine the statistical distribution of temperature, and the heat transfer performance of randomly packed spherical fuels. Figure 1.1 illustrates the conceptual design of the suggested wireless device in the packed-bed system. We call a single device a "wireless pebble."

The wireless pebble has numerous potential applications, such in a packed pebble-bed for the FHR in extensive scaled research experiments. Scarlat discussed the alternative of using 'Dowtherm A' instead of FLiBe, the molten salt coolant used in FHR, by pointing out that both coolants match the Prandtl number in a specific temperature range [2], [7], as shown in Figure 1.2. If one can match its Reynolds number easily in a scaled experiment, the use of Dowtherm A between approximately 57 °C and 87 °C is an alternative to the temperature range of 600-700 °C of FLiBe its normal operation. As the wireless module can operate properly below 85 °C, the maximum operational criterion of an electric circuit, our suggested wireless device both measures local temperatures non-invasively and helps

the statistical analysis of heat transfer in scaled experiments of packed pebble-beds for FHRs.

In this paper, the development and validation of a non-invasive wireless device for pebble-bed temperature measurements will be described. These suggested devices may offer a powerful approach to investigating heat transfer coefficients in a non-invasive manner and designing randomly packed configurations for further studies.

4
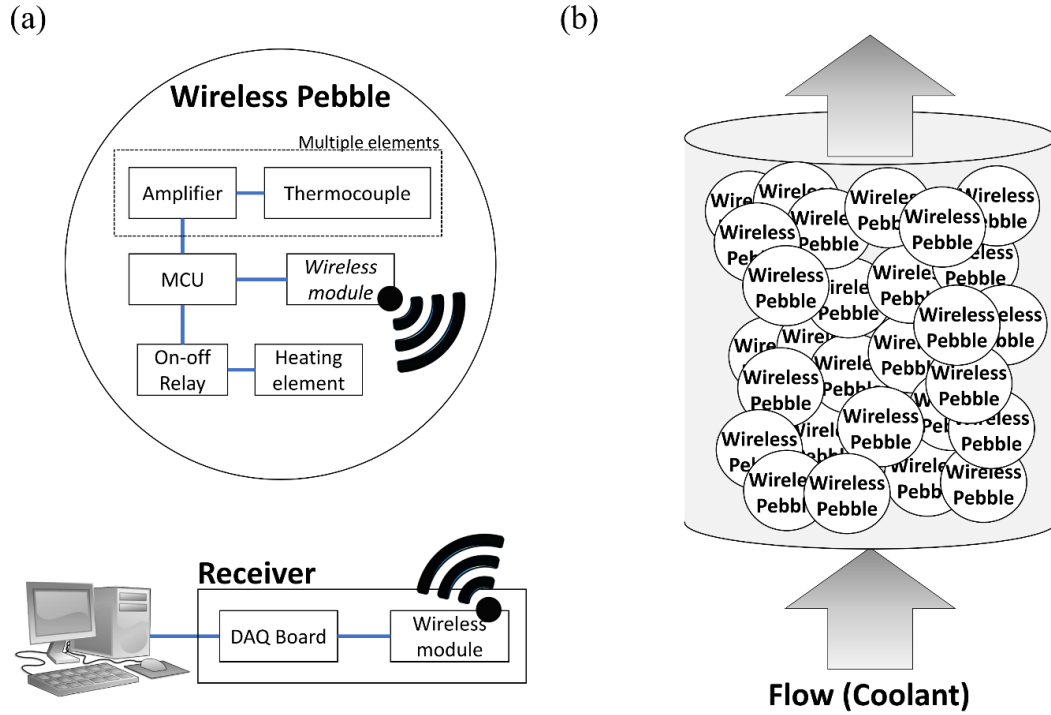
Figure 1.1 Conceptual design of the proposed pebble experiment adopting a wireless communication method: (a) Block diagram of the wireless pebble and receiver. A single wireless pebble should contain the main circuit module, wireless module, sensor modules, and internal heater module. The receiver has a wireless module and can receive data from each wireless pebble. (b) The experiments with coolant flow use multiple devices for wireless measurement.
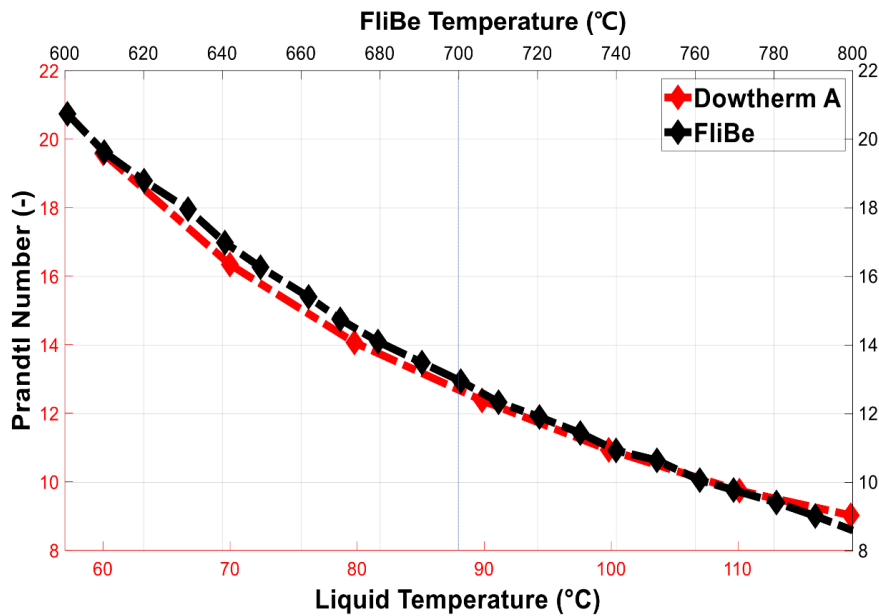
Figure 1.2 Prandtl numbers of FLiBe and Dowtherm A at various temperatures [4].

1.2 Machine learning-aided nuclear accident diagnosis research

A loss of flow accident (LOFA) is a design-based accident that causes a loss of designed reactor coolability due to pump failure during operation. In recent years, an increasing number of studies have been conducted to analyze nuclear accidents with machine-learning technology [17]–[23]. In the field of fault diagnosis for nuclear power plants, operational support systems with artificial intelligence have been developed to help operators mitigate failures. Specifically, fuzzy logic techniques for predicting failure scenarios in nuclear systems [21], [24], and probabilistic support vector machines (SVMs) for monitoring the state of components in nuclear power plants [23] have been studied. Kim et al. (2015) used an SVM to classify break position and size in the case of loss of coolant accidents. Fernandez et al. (2017) used an artificial neural network (ANN) with multiple sensors to evaluate the ability to predict system behavior during various core power inputs and a LOFA. Machine learning has also been used to advance the prediction of various two-phase flow phenomena, including flow-regime transitions [25], the modeling of pressurization in a PWR by ANN [26], and critical heat flux (CHF) predictions [27].

Recent advances in machine learning suggest it can be applied to unprotected LOFA analysis and prediction. As a first step, this study used an SVM and transient reactor outlet temperature input to investigate the predictability of loss of reactor core flow upon a reactor pump outage. The results, in terms of predictability, address the possibility of establishing a relationship between flow change and readily measurable reactor core outlet temperature. This, in turn, implies the feasibility of advanced accident diagnosis by removing the traditional boundary between different, yet strongly correlated, physical quantities. As a

6

next step, the author used an SVM to investigate the correlation between local fuel temperature (i.e., peak cladding and centerline temperature) and reactor outlet temperature during an unprotected LOFA. The author then explored the predictability of unmeasurable local temperature using readily measurable temperatures, advancing the predictability of reactor core damage during a LOFA. This study represents an initial attempt to remove the boundaries between different physical quantities (i.e., change in flow rate and core outlet temperature), and between different locations (i.e., local fuel temperature and core outlet temperature) during a LOFA.

In this study, reactor core outlet temperature, T_{out}, is the primary parameter of interest. With constitutive models, obtained transient T_{out} (t) can be seen as an outcome of continuity, momentum, and energy balance, which are related to the transient flow change, $\dot{m}_{in}$ (t), and local temperature information T_{local} (t), such as the fuel peak temperature, as illustrated in Figure 1.3.

The relationship between T_{out} (t) and $\dot{m}_{in}$ (t) is not straightforward; the energy transfer rate from fuel to coolant during transient flow is affected by the energy deposition rate on the fuel structures. Energy transfer during transience is determined together with continuity and momentum, all of which are coupled to constitutive equations and correlations. Nuclear system codes such as RELAP5-3D and MARS mechanistically solve these coupled equations in a forward direction, as shown in Figure 2. Accident diagnosis tackles the problem in the opposite direction by using a measurable response parameter, T_{out}, to find the cause of the transience, $\dot{m}_{in}$ (t). This reversed process can best be executed by finding the inverse operator of the forward process.

7
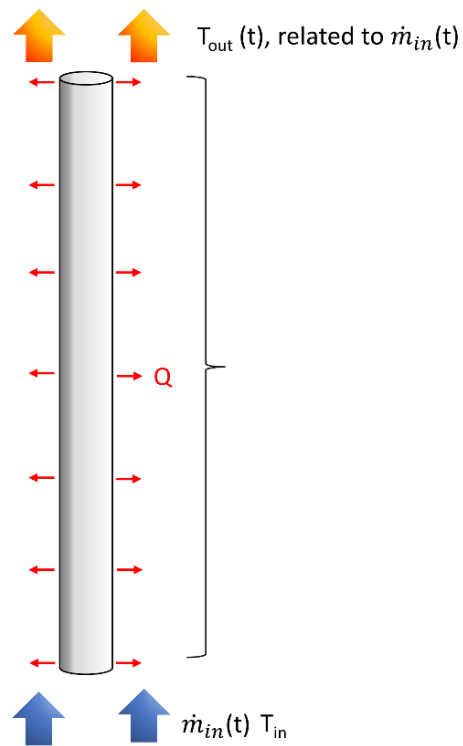
Figure 1.3 Significance of T_{out} during a LOFA resulting from $\dot{m}_{in}$ (t)
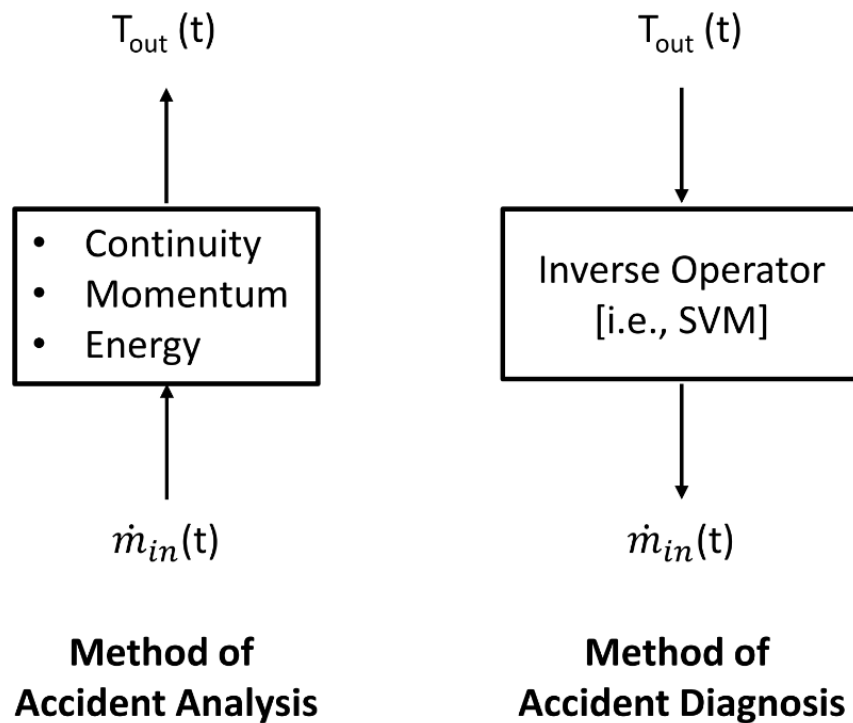
Figure 1.4 Schematic of a typical accident analysis method, and an accident diagnosis method

In this study, the author obtains the inverse operator by training an SVM with the change in $\dot{m}_{in}$ (t) and the T_{out} (t) obtained from a MARS simulation. T_{out} (t) is chosen as the primary response parameter of interest because it contains information for the transient loss of flow and is a readily measurable parameter during reactor accidents.

1.3 Research objective and thesis organization

In this study, the author attempts to transfer new technologies from other fields to nuclear engineering, such as wireless devices and machine learning. Through the application of these new technologies, a heat transfer experiment using wireless communication and a possible accident diagnosis process using machine learning are described.

The thesis is organized as follows. Chapter 2 and Chapter 3 cover the development and verification of wireless pebbles, and Chapter 4 and Chapter 5 present a machine learning-aided case study, pressurized water reactors (PWR) pin. Lastly, Chapter 6 discusses the importance and implications of this paper.

2. Design and development of the wireless device for scaled FHR experiments

In this chapter, the design and development of the wireless pebble are described. The wireless device requires specific design conditions. Each wireless pebble has the following requirements:

1) Measured temperatures can be transmitted wirelessly.

2) The surface temperature of the all circuits must remain at a temperature below 85℃.

3) All modules should be small enough to be enclosed inside the wireless device.

4) The internal heating element should be capable of heating uniformly to a constant power over the surface.

The cover of the wireless pebble is made of thin metallic steel with a spherical shape. This is beneficial for the heat transfer between the inside and the outside of the pebble. A fabric-based internal heat source to supply constant heat inside the device is considered. This method has the advantage of easily calculating power by using the voltage and resistance across the heating element.

2.1 Pebble components

2.1.1 Main circuit module

Each wireless device basically requires a wireless module, a programmable microcontroller unit (MCU), and peripherals for temperature measurement, such as TCs and their amplifiers. While TCs measure temperatures as small levels of voltages, their amplifiers digitize the temperature signal and convert it into a readable format compatible with serial peripheral interface (SPI) relay.

10

Each MCU in the wireless device is programmed to obtain temperature information converted to readable format and transmit this information to the designated receiver through the wireless module. Each receiver has a wireless module capable of collecting informative data from up to five individual wireless devices, which are finally exchanged via RS232 input to the PC and stored in the data acquisition (DAQ) system. Multiple receivers can collect data from multiple wireless devices. The Arduino Pro Mini (3.3V), a smaller version of the embedded ATmega328 (Appendix A.4) at approximately 18 x 33 mm, was adopted as the main MCU to reduce the final size of the wireless device.

2.1.2 Wireless modules

Wireless communication has become an essential technology for portable devices such as smartphones, tablet PCs, and laptops. It transmits information or power between two or more nodes connected by an electrical conductor. The radio wave is the most common wireless technology, and there are many allowable distances from a few meters to hundreds of kilometers. The nRF24L01 module, an ultra-low power integrated circuit from Nordic Semiconductor (Appendix A.1), was selected because it is small, low-power, SPI-compatible, and can transmit and receive on the worldwide 2.4–2.5 GHz ISM band. Additionally, the ShockBurst™ technology embedded in the nRF24L01 provides automatic response, transmission, and reception of up to 32 payload bytes to the device.

As the number of wireless devices increases, it is crucial to carefully consider how to configure important data packets. This is because the configuration can affect the high reception rate of data packets between each wireless device and the receiver.

Each wireless device has a unique pebble identification number (ID) and transmits information about its six different inner surface temperatures to the receiver using the

11

nRF24L01. Because the nRF24L01 module can send only 32 payload bytes of data at a time, the length of the data packet sent from a single device is limited to 32 bytes. The detailed configuration of the data packet protocol for the wireless pebble is shown in Table 2.1. Unlike the data packet configuration of the transmitter, that of the receiver includes the time at which the packet arrived on the basis of receiver time. This is to identify the order in which packets from different wireless pebbles arrive. Thus, the received data from the various pebbles are easily identified based on the time received at the receiver.

Each set of temperature data is displayed up to the first decimal point. For the user's convenience, each temperature value is multiplied by 10, and then converted to a hexadecimal value that occupies only 3 bytes. For example, if the first piece of temperature data is 25.7 °C, it is converted to 257, and $257_{10} = 101_{16}$. Likewise, if the second temperature is 42.7 °C, it is converted to 427 and $427_{10} = 1AB_{16}$, and then the corresponding hex value is 1AB. If the measured value exceeds FFF_{16}, it is fixed to FFF16 and maintains its data size, 3 bytes.

2.1.3 Sensor module

To measure the temperatures, many bundles of 5TC-GG-K-36 (Appendix A.5) type K insulated TCs were chosen. Each TC could measure the temperature from -200 °C to 700 °C with an accuracy of ±2 °C. As the TC's electromotive force is small and sensitive, an amplifier was used to identify the measured temperatures. The amplifier for the TCs, the MAX31855K breakout board from SparkFun, was selected (Appendix A.2). The breakout board digitizes the temperature value and sends it to the other side via the SPI interface.

Table 2.1 Configuration of data packet protocol for each wireless pebble. (a) Transmitter data packet (b) Receiver data packet (c) Temperature data packet in transmitter and receiver

(a)

Contents	Start code	Delimiter	ID	Delimiter	DATA	Check sum	Delimiter	End code
Number of bytes	1	1	1	1	24	1	1	1
Data type	Char	String	Char	String	Char & String	Char	String	Char
Value	0x02	,		,			,	0x03

(b)

DATA						
Contents	TC #1	Delimiter	TC #2	Delimiter	…	TC #6	Delimiter
Number of bytes	3	1	3	1	…	3	1
Data type	Hexa Char	String	Hexa Char	String	…	Hexa Char	String
Value		,		,	…		,

(c)

Contents	Start code	Delimiter	ID	Delimiter	DATA	Check sum	Relative Time	Delimiter	End code
Number of bytes	1	1	1	1	24	1	-	1	1
Data type	Char	String	Char	String	Char & String	Char	String	String	Char
Value	0x02	,		,				,	0x03

2.1.4 External induction heating

Initially, induction heating was considered as the heating method. It is a method of heating a metal object by using electromagnetic induction. When a current is supplied to a coil, an eddy current is generated on the surface of a shallow metal sphere, raising its surface temperature. The induced heat is not constant on the spherical surface but can be used for preliminary tests to check the influence of the induced heat and the operation of the wireless module. A module with a 1000-watt, zero voltage switching (ZVS), low-voltage induction heating board and wound coils induced heat successfully.

2.1.5 Internal heater module

Although external induction heating does not generate heat uniformly, an induction heating element inside is free from this limitation. To generate uniform heat on the surface of the pebbles, a fabric-based heating material made by WireKinetics Corp. was used (Appendix A.3). The fabric module was made with textile-type micro-metal conductive (MMC) yarn fibers. As shown in Figure 2.1(a), the fabric heating material is composed of micro-metal lines and many polymer yarns. It has 0.9–4.0 ohms/meter of electric resistance. The pitch range of the MMC fibers can be defined from 2 mm to 100 mm, and the performance of the heating fiber is determined by the pitch. The fabric heating material broadly covers the S-shaped micro-metal (Figure 2.1(b)) to help distribute heat in a uniform way and is internally attached inside the surface of the two hemispheres. The heating material requires a 3.5–12 V DC power supply. The heating pad is equipped with a yellow sticker, which is an insulation film called polyimide (PI). This film maintains close contact between the heating material and the inner surface of the pebble to reduce contact resistance, as shown in Figure 2.1(c).

14
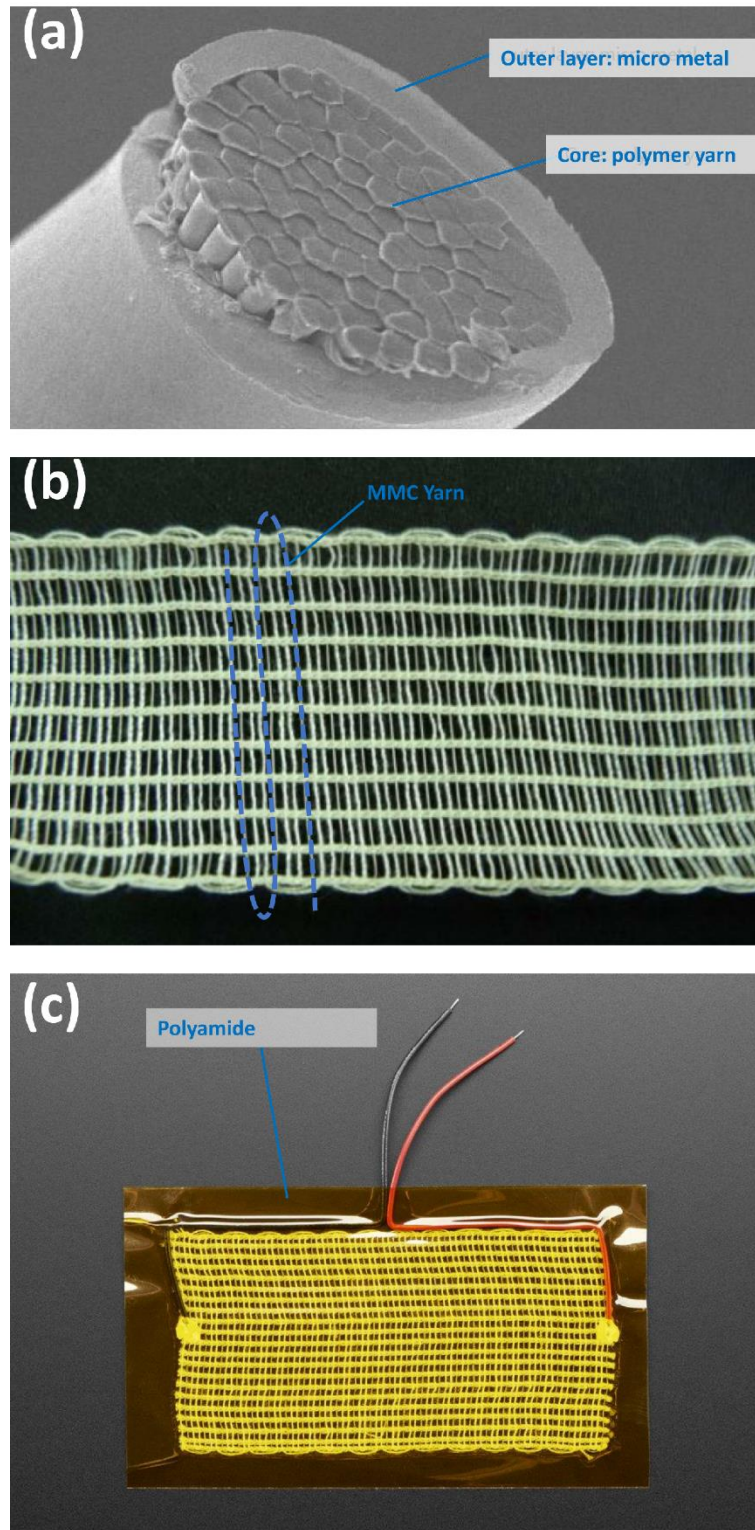
Figure 2.1 (a) Micro metal conductive (MMC) yarn (b) Heating fabric knitted by MMC yarn (c) Heating pad with film polyimide (Appendix A.3)

2.1.6 Software architecture

This section discusses software architecture. First, the Arduino-based C++ script is uploaded to the MCU, and the classes used in the script are used in both the receiver's script and the GUI application. This is to integrate into one source code. The overall software layer category is divided into three major categories. 1) Device management (serial communication); 2) Data receiver controller by produce-consumer design pattern; 3) GUI application (data saving and settings). The PC GUI is designed to receive data from more than 100 wireless pebbles.

In Figure 2.2, Class *basepacket* is a class that can receive data using the packet described above, and the wireless device class is an interface implemented by using the concept of inheritance within this base packet class. Class *wirelessdevice* has two child classes, one for the wireless receiver and one for the wireless transmitter. Thus, one complete program is in Arduino-based C ++ on ATmega 328P, and a wireless receiver class is included with the GUI programs in C# and LABVIEW. The produce-consumer design pattern, which is a commonly used design pattern, is used in this GUI program, which provides a way to manage data effectively. This pattern is helpful for managing external data from, such as that transmitted by serial communication.

16
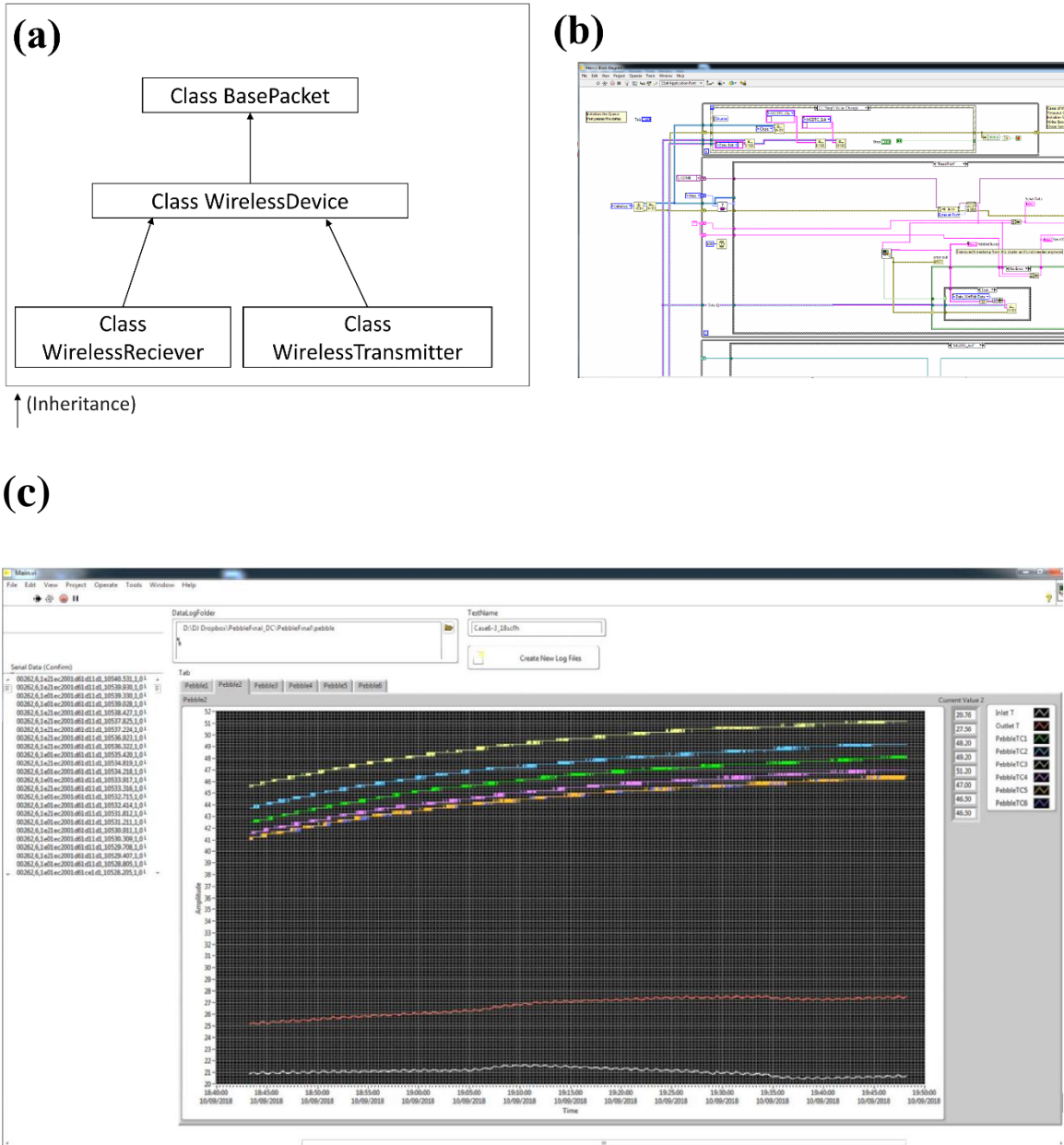
Figure 2.2 **(a) Basic software architecture native to ATmega328P, Arduino-based C++ (b) Produce-consumer design pattern (C#, LABVIEW) (c) GUI Applications**

2.2 Wireless pebble assembly

2.2.1 First prototype

The first prototype of the wireless pebble was developed as shown in Figure 2.3. This device is designed to check the normal operation of components or confirm the basic functions through a combination of commercial products. The commercial products include 1) the smallest MCU, the ATMega328 Pro Mini, 2) The radio frequency (RF) module nRF24L01, a wireless module, 3) MAX31855K TC amplifier, 4) two TCs. The two TCs were attached first to measure the temperature inside and outside the surface. In the following sections, several simple preliminary experiments on the three wireless pebbles are presented.

2.2.2 Final prototype

In the first porotype, most of the modules or components were connected by wires. However, a more compact design was required to increase the number of temperature measurement points on the wireless pebble. However, due to the limited space inside the sphere, the wireless pebble needed to be miniaturized. Also, because the structure measured temperature at only two points that were not symmetrical, marble gravel could cause some spatial errors when used in gravel packing systems. For this reason, a wireless pebble was designed to be smallest in size after having a single customized circuit system capable of measuring up to six temperatures. Figure 2.4 shows a customized circuit prototype (one-board system) that includes an MCU, six TC amplifiers, and a socket for inserting an RF module, etc. TC #1 to TC #6, shown in Figure 2.4 (a), are sockets designed to plug in and fix 6 TCs.

18
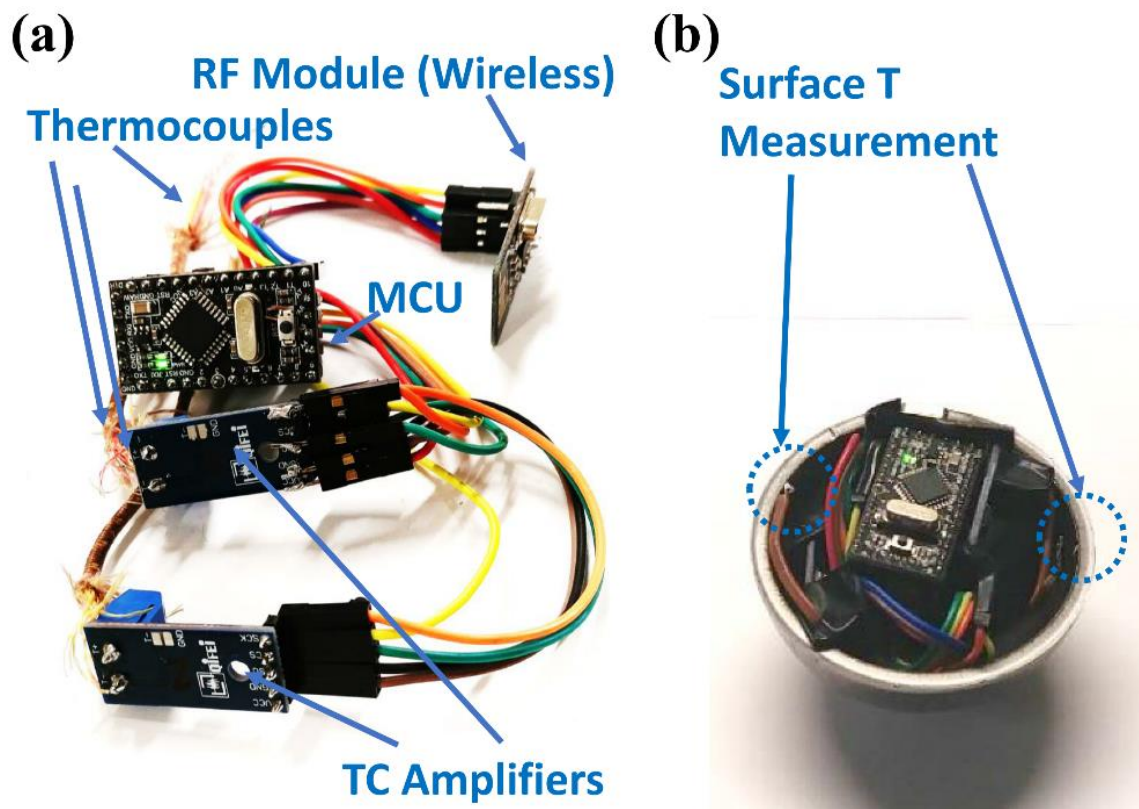
Figure 2.3 First implementation of a wireless pebble. Two thermocouples (TC) are used to obtain the surface temperatures of the pebble
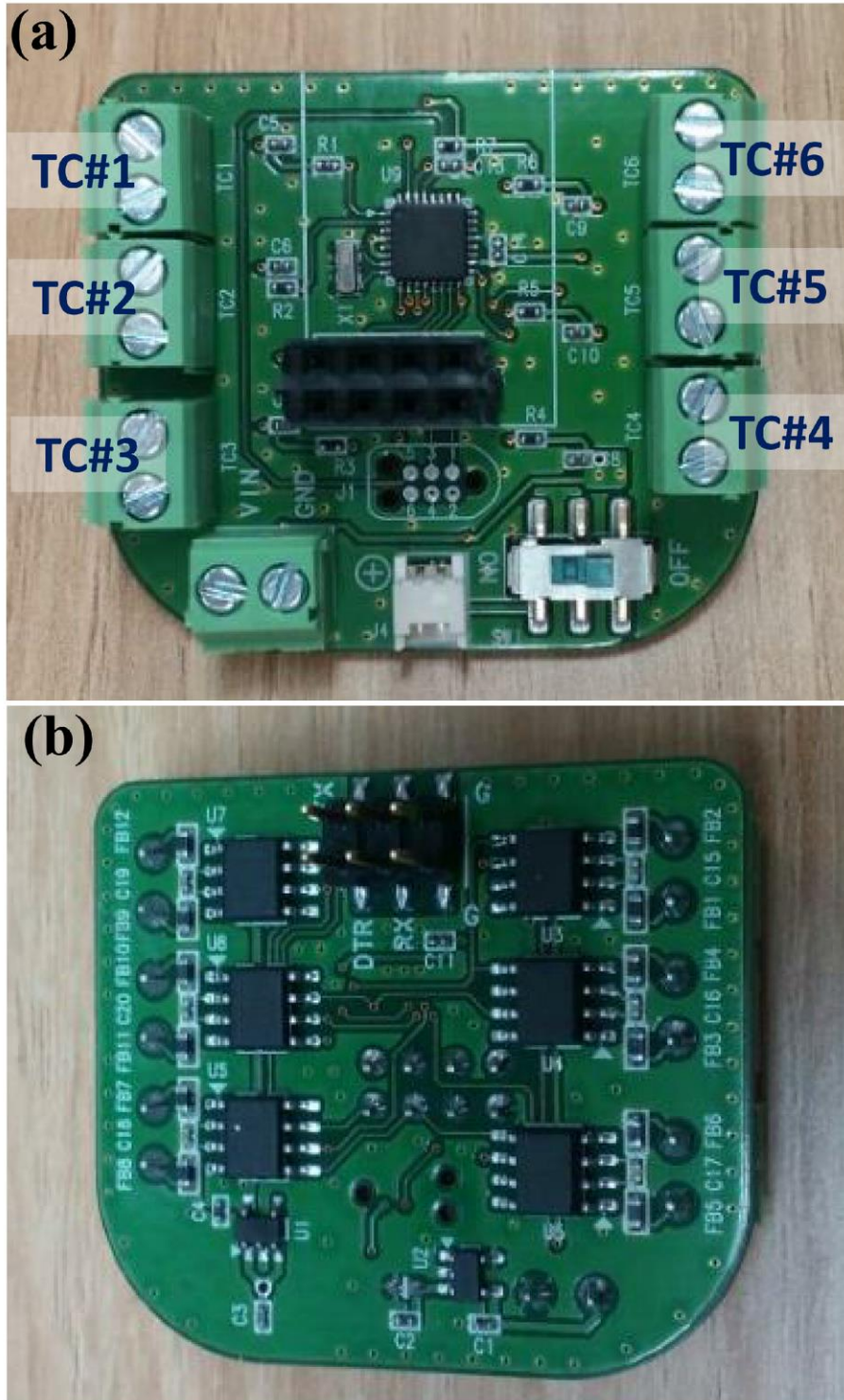
Figure 2.4 Customized circuit prototype (one-board system). (a) Front (b) Rear
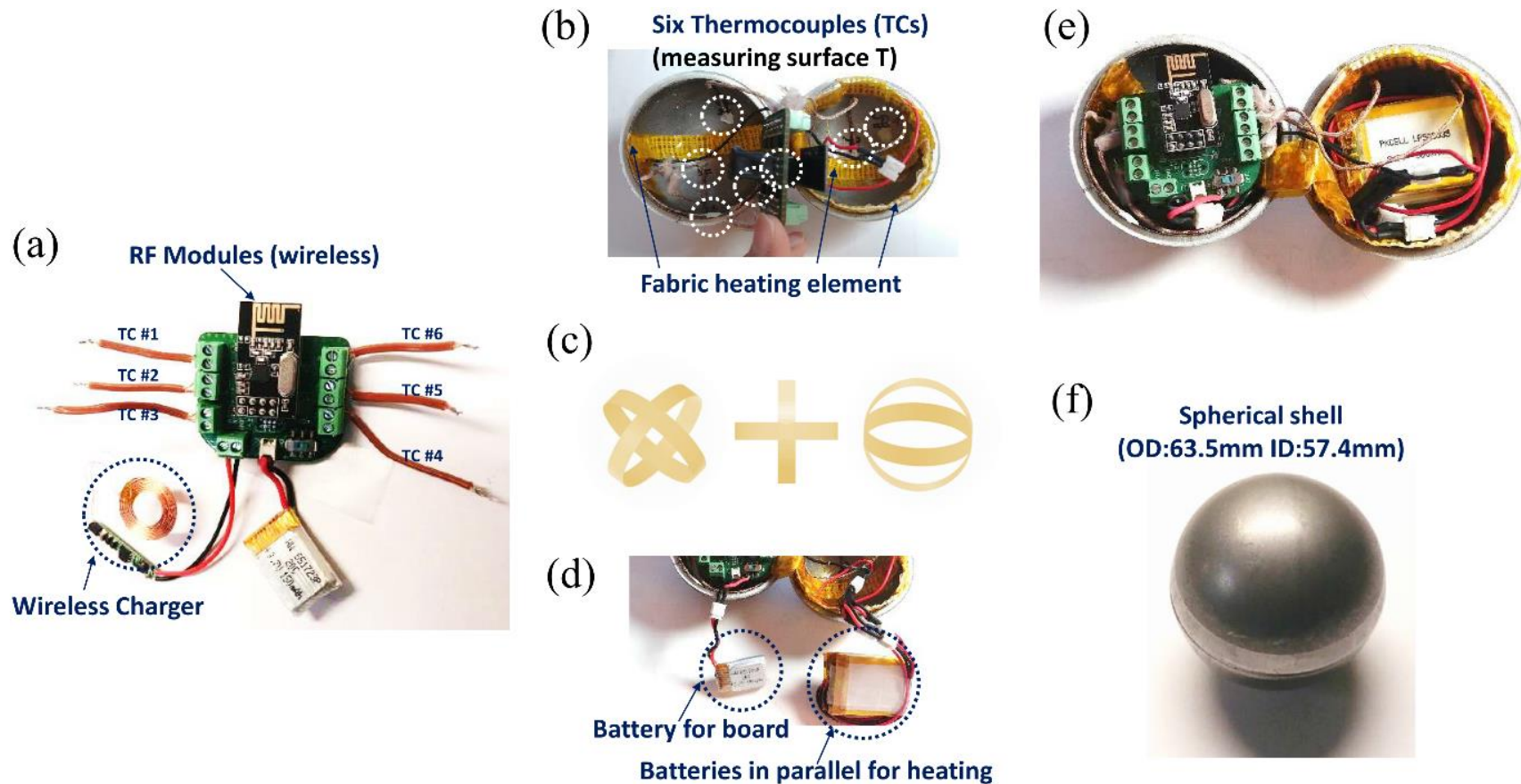
Figure 2.5 Wireless pebble assembly. (a) The ATmega328P-based customized printed circuit board (PCB) includes all the circuits of the wireless pebble. The RF modules nRF24L01 are mounted on the customized board, and six measurement TCs and wireless charger modules are connected to the board. (b) The six thermocouples attached on the inner surface of the shell sphere can measure six different points on the surface. The internal heater attached to the inner surface of the sphere is the fabric heating element. (c) This inner heater forms a vertical crossing of the two bands in a symmetrical manner. (d) Two different purposes of the battery are related: 1) operating all circuits, and 2) operating all stacks in parallel for the internal heating element. (e) The top view of the wireless pebble, with all the modules fitted properly in the two stainless steel hemispheres. (f) The wireless pebble assembly has an outer diameter of 63.5 mm and an inner diameter of 57.4 mm

Figure 2.5 shows the fabricated board and its assemblies. For a compact design, the circuits in all the modules, such as ATmega328 and the amplifier, were combined and customized, mounting the RF module nRF24L01. The program modules for the robust wireless communication of multiple pebbles were designed and tested. In Figure 2.5(a) and (b), the six TCs TC#1 to TC#6 are attached at six different inner surface locations of the wireless pebble. The optional function of the wireless charger is designed to charge the battery effectively. The internal heater forms a vertical crossing of two bands so as to be as symmetrical as possible, as shown in Figure 2.5(c). The first Li-polymer battery for operating all circuits is connected to the fabricated board, and the secondary Li-polymer battery, stacked in parallel with the internal heating element, is inserted into the remaining space inside the sphere (Figure 2.5(d)). In essence, the cover of the wireless pebble, consisting of two hemispherical shells, is intended to be made of stainless steel for its high thermal conductivity. Figure 2.5(e) shows that the fabricated board, TCs, and batteries are well-placed inside the shell of the sphere. Finally, when this part is combined with the sphere, the outer diameter of the sphere is 63.5 mm and the inner diameter is 57.4 mm, as shown in Figure 2.5(f).

2.3 Preliminary experiments for verifying basic functions of wireless pebble

2.3.1 Verification experiments for single wireless pebble and two pebbles under induction heating

The purpose of these experiments is to examine the measurements and the wireless communication of the wireless pebbles under induction heating or internal heating. Figure 2.6 represents the experimental setup for three wireless pebbles placed on an element under induction heating. The covers of the three prototypes in Figure 2.5 were closed, and the

prototypes were placed on the induction coil of a commercial induction heater. This section focuses on verifying the rise in temperature, and whether the data transmission through the receiver operated normally.

Two measurement points inside and outside the shell of each pebble were used to determine how much heat was generated by the thin shell. The test condition varied the input voltage of the inductive power supply from 12 V to 16 V. Figure 2.7 and Figure 2.8 show the temperature change of single wireless pebbles, and the result of using two wireless pebbles, respectively. Both devices used the same inductor coil, but the steady-state temperature was different.

23
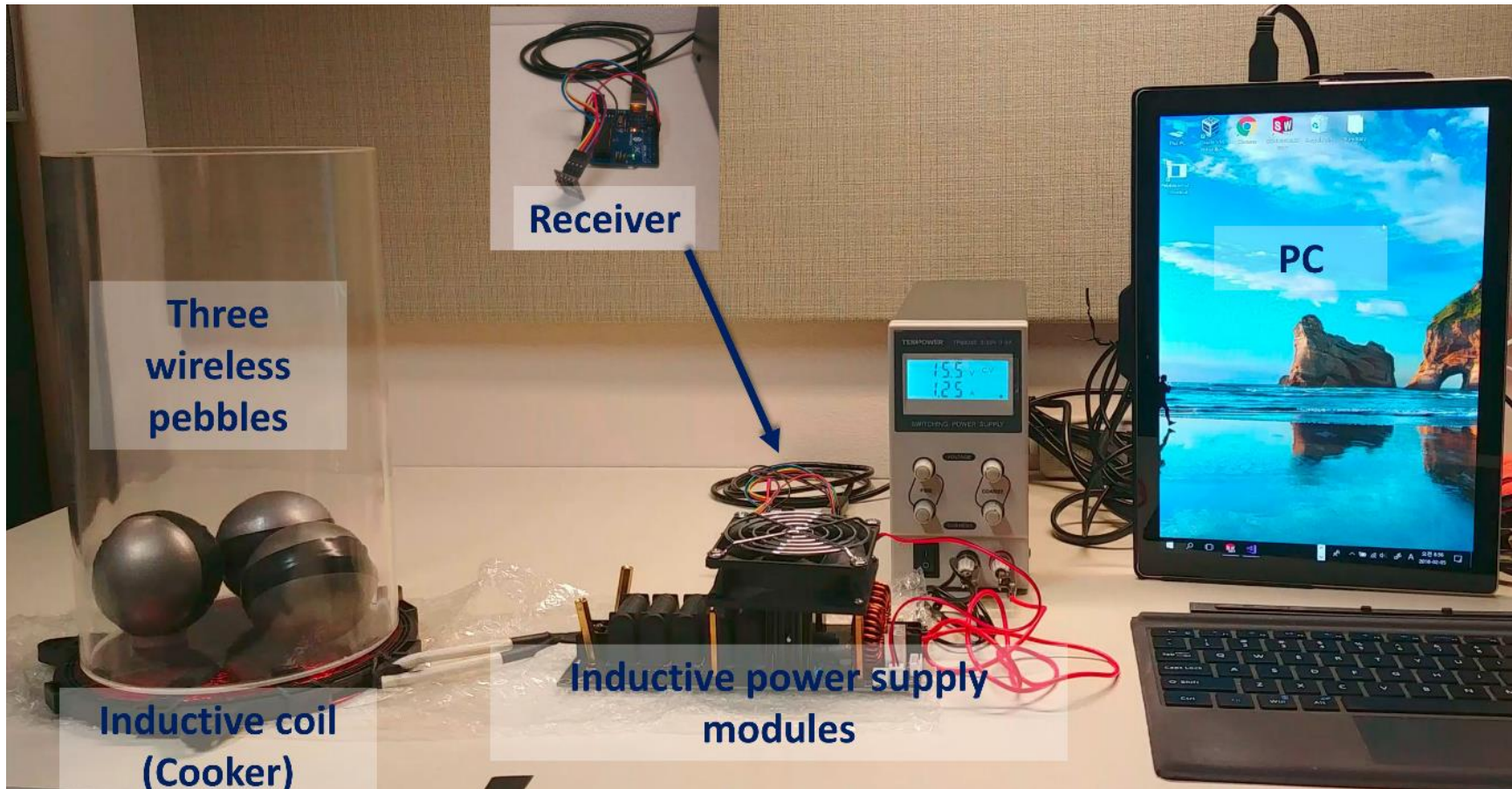
Figure 2.6 Experimental setup for collecting temperature data wirelessly under induction heating
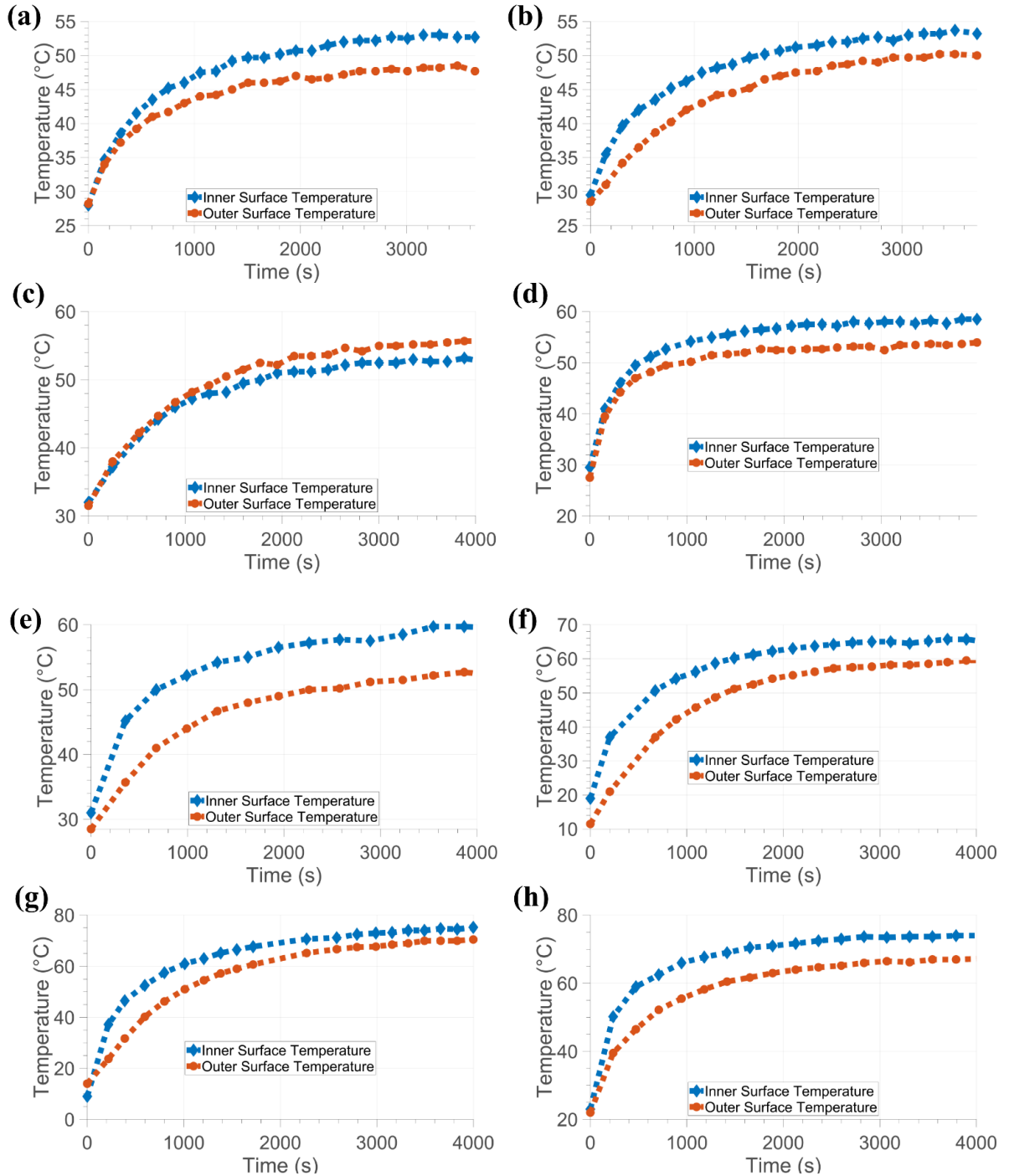
Figure 2.7 Trends in temperature data received from a surrogate pebble. Conditions: (a) 12 V, 0.49 A, 28 °C external temperature, (b) 12 V, 0.48 A, 29 °C, (c) 13 V, 0.53 A, 27 °C, (d) 13 V, 0.53 A, 32 °C, (e)14 V, 0.49 A, 27 °C, (f) 14V, 0.57 A, 27 °C, (g) 16 V, 0.66 A, 28 °C, (h) 16 V, 0.66 A, 32 °C

25
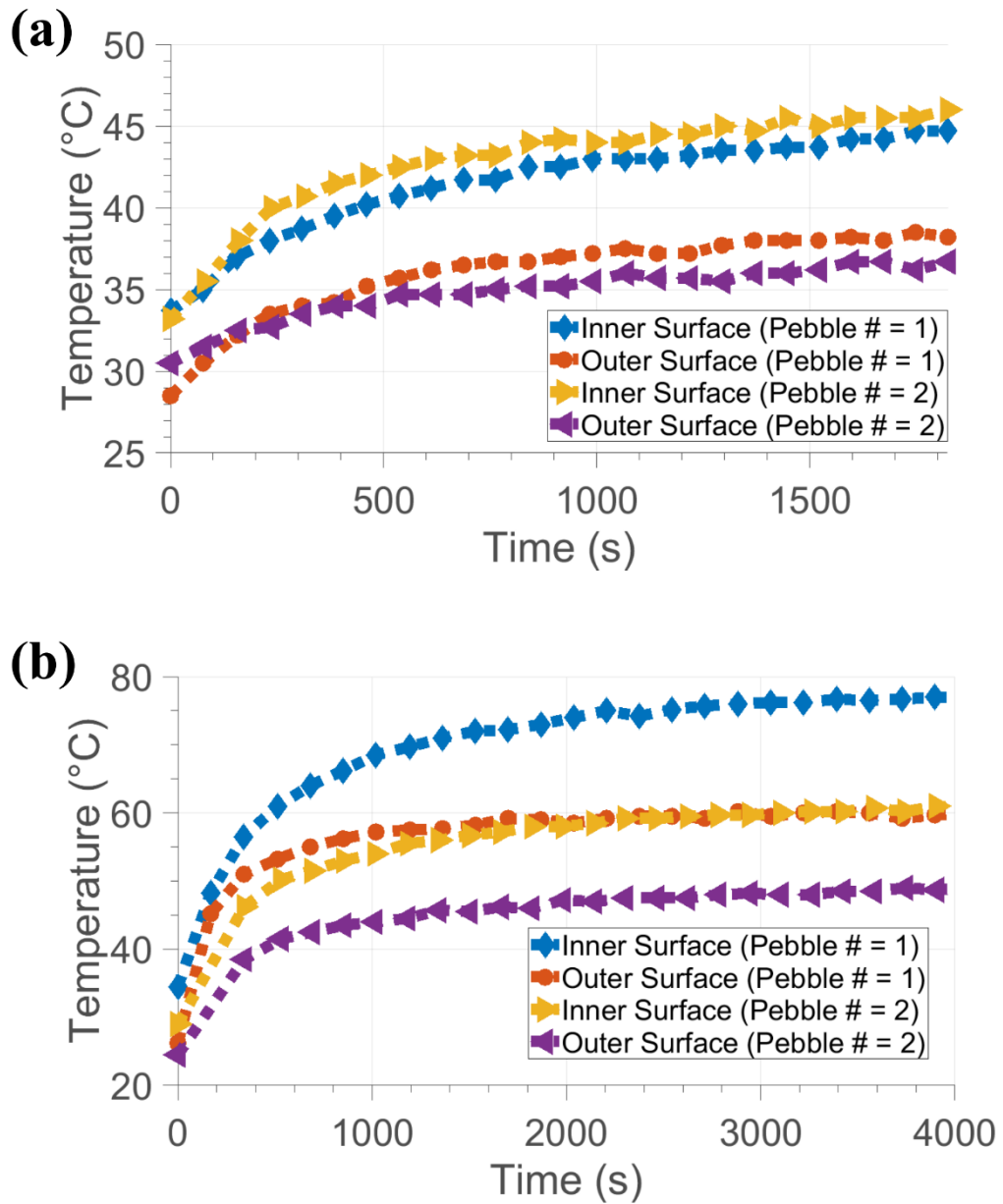
Figure 2.8 Trends of temperature data from two surrogate pebbles with induction heating: (a) 15 V, 0.49 A, 27 °C of external temperature, (b) 18 V, 0.48 A, 28 °C

The heating power induced by induction heating was estimated for both conditions in the above experiments. The estimated power provided a baseline for the thermal energy that each wireless pebble had versus the voltage provided by induction heating. There were two methods used: 1) calculating with the assumption that the ball is heated by natural air convection, 2) calculating the heat exchanged through the conduction of stainless steel.

Using the air thermal properties and Nusselt number equations correlated in Table 2.2, the Nusselt number and the heat transfer coefficient were first derived, and the heating power (Q) divided by the cross-sectional area was calculated to obtain an estimation of the magnitude of the heating induced through induction in one wireless pebble, as shown in Figure 2.9.

From these preliminary results, it was concluded that it would be difficult to prove the uniformity of heating power for the situation where the wireless pebble is placed in different positions in space. Two heating methods, induction heating, and internal fabric-based heating were considered to provide remote heating for the pebbles.

Table 2.2 (a) Thermal properties of air measured as temperature changes (density, specific heat, thermal conductivity, kinematic viscosity, expansion coefficient, Prandtl number) (b) The Nusselt number equation of air in natural convection

(a)

Temperature	Density	Specific Heat	Thermal Conductivity	Kinematic Viscosity	Expansion Coefficient	Prandtl Number
T (^{o}C)	ρ (kg/m^3)	Cp (kJkg^{-1}K^{-1})	k (Wm^{-1}K^{-1})	v×10^{-6} (m^2/s)	b×10^{-3} (K^{-1})	-
20	1.205	1.005	0.0257	15.11	3.43	0.713
40	1.127	1.005	0.0271	16.97	3.2	0.711
60	1.067	1.009	0.0285	18.9	3	0.709
80	1	1.009	0.0299	20.94	2.83	0.708

(b)

Nusselt number correlation	Applicability
$Nu = 2 + \dfrac{0.589\mathrm{Ra}_D^{0.25}}{\left(1 + \left(0.469/\mathrm{Pr}\right)^{9/16}\right)^{4/9}}$	$\mathrm{Pr} \geq 0.7$ $Ra \leq 10^{11}$

(a)
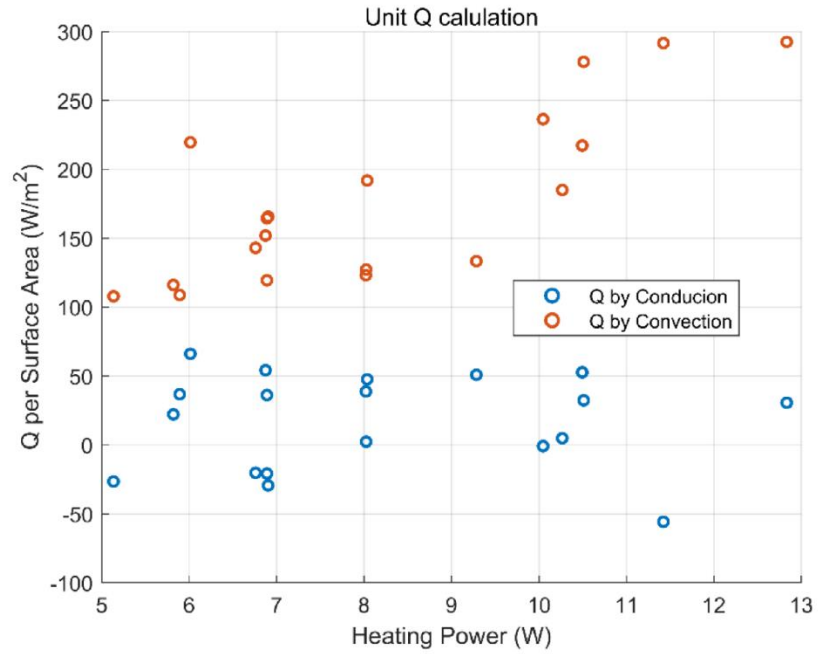
(b)
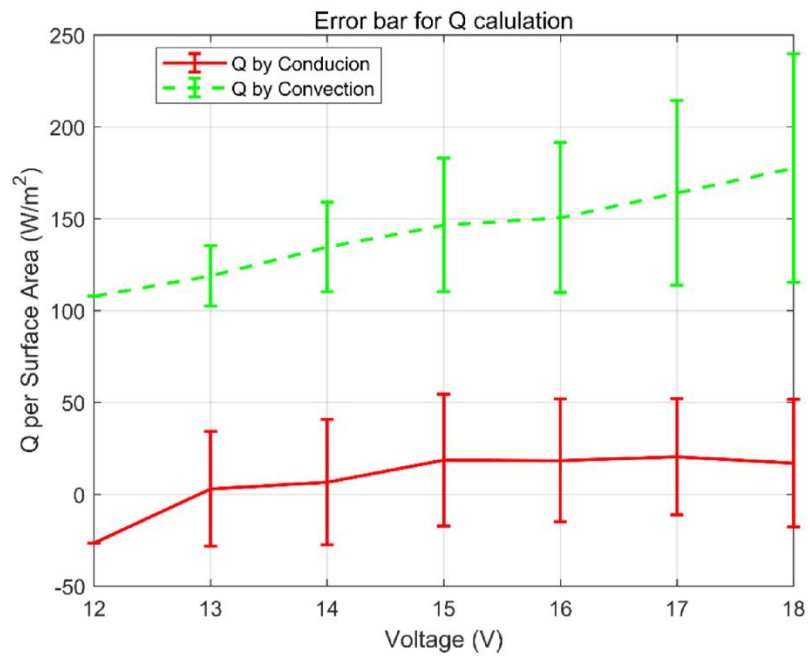
Figure 2.9 (a) Comparison of heating power per surface area by conduction (red) and convection (blue). (b) The input voltage of induction circuit and the trend in heating power per surface area

2.3.2 Verification experiments for three wireless pebbles under internal heating

In fact, an inductor does not provide uniform heat over the surfaces of the spherical pebbles because of the non-uniform magnetic field affecting the metallic shell. Even if the induction heater provided a nearly uniform current to the shell structure, there are more difficult problems to resolve. If the shape of the inductor coil is changed to another type, such as a flip type or a spiral type, all the components surrounding the inductor should be changed. The capacity of the power supply and the current provided to the coil will be changed as the design of the inductor coil as well.

In this experiment, fabric heating was used to heat three wireless pebbles. The graph in Figure 2.10 shows the peak in the time range between 200 s and 500s. The "ID = 1" means the first pebble ID, and "Inner" and "Outer" indicate the inner and outer surface temperature of each wireless pebble. After the pebbles reach their peak temperature, the 3.7 V battery in the pebbles all seemed to be fully discharged. The estimated resistance of the fabric heater is approximately 10 ohms. If the 7.4 V battery is used, 740 mA of current flows in the fabric heating material, which means that a 150 mAh Li-polymer battery would last 720 s (12 min), approximately. Considering the internal resistance, the lifetime of a 7.4 V battery would be less than 720 s.

In the case of using a fabric-based heating pad, supplying uniform heat flux from the inner side of the sphere surface is possible. In addition, one can easily estimate the amount of heat generated from the heating pad because the electric resistance of the fabric material is measurable, and the amount of current can be calculated. Because the fabric material is a metal material, its resistance is proportional to its length and cross-sectional area. In Table 3, the parameters related to battery life are listed. Increased resistance of the heating pad

30

leads to increased battery time. As expected, using a larger capacity battery ensures more battery time.

Therefore, it is very important to increase the run time by connecting the batteries in parallel as shown in Figure 2.5 (d). In the experiment described in the next chapter, three 500 mAh batteries are connected in series and used as power for internal heating. In this case, a battery lifetime of at least one and a half hours is guaranteed.

Table 2.3 Expected lifetime of batteries as relevant parameters

Voltage (V)	Fabric Resistance (Ω)	Total Resistance (Ω)	Total Current (A)	Consumed Power (W)	150 mAh of battery lifetime (min)	500 mAh of battery capacity
7.4	7	7	1.06	7.82	4.26	14.2
7.4	9.2	9.2	0.80	5.95	11.19	37.3
7.4	13	13	0.57	4.21	15.8	52.7
7.4	21	21	0.35	2.61	25.5	85.1
11.1	7	7	1.59	17.6	5.68	18.9
11.1	9.2	9.2	1.06	13.4	7.46	24.9
11.1	13	13	0.80	9.48	10.5	35.1
7.4	7	7	1.06	7.82	4.26	14.2
7.4	9.2	9.2	0.80	5.95	11.19	37.3
7.4	13	13	0.57	4.21	15.8	52.7
7.4	21	21	0.35	2.61	25.5	85.1

Figure 2.10 Graph showing trend of temperature data received from three wireless pebbles

3. Validation of wireless device for scaled FHR experiments

In this section, the local heat transfer coefficients of the developed wireless pebble are calculated with an airflow heat transfer experiment and compared with values in the literature. Many research projects [3], [4], [11] have actively studied Nusselt numbers in different heat transfer environments. Because these studies are based on various correlations, the heat transfer coefficient attained from each correlation equation can be compared with the local heat transfer coefficients computed from our experimental apparatus by measuring the surface temperatures of the wireless pebbles. The validation process for a single pebble relies on 1) the airflow rate of change, 2) the location of the TC attachment, and 3) the orientation of the internal heater, 4) the heat transfer coefficients in multiple wireless pebbles are subsequently demonstrated. The validation process results will be extended to multiple wireless pebbles in future packed pebble-beds.

3.1 Experimental Setup

A heat transfer experiment with air flowing over the sphere of the pebbles was conducted to validate the feasibility of the wireless pebble. In the test facility, as shown in Figure 3.1 (a) and (c), the air flows along a vertically erected cylindrical tube, from the bottom inlet to the top outlet, at a controlled volume flow rate while the wireless pebble located between flange 1 and flange 2 is placed in order to estimate the local heat transfer coefficient through wirelessly collected pebble temperatures. Also, the heating element inside the wireless pebble, which heats the surface of the pebble and increases the temperature of the outlet, creates heat transfer between the surface and the air flowing from the inlet to the outlet.
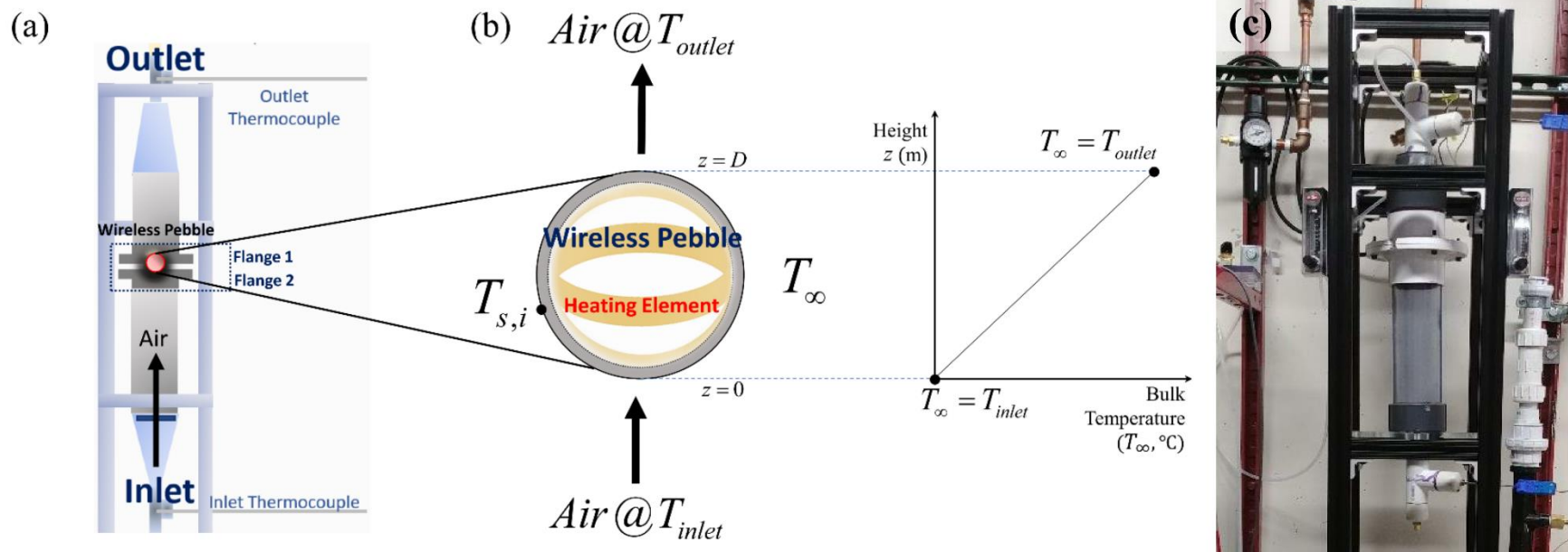
Figure 3.1 (a) Overall heat transfer experiment configuration of the air flowing over a single wireless pebble (b) Simple model for heat transfer through energy-balanced equations (c) An installed experimental facility

When the heat transfer flow reaches a steady state, the increased temperature of the outlet of the plant is gradually balanced by this heat transfer process. The following Eq. (3.1)–(3.5) relating to the local heat transfer coefficient h are determined by the energy balance equation in a steady state. Here, the bulk temperature T_∞ is simply assumed to change linearly in relation to z, which is the distance from the bottom of the wireless pebble in the direction of airflow. Full insulation of the facility helps to ensure the heat energy produced by the wireless pebble is converted into increased air temperature at the outlet.

Because the temperature of six inner surfaces is measured directly at the position of attachment of the six TCs in the wireless pebbles, the corresponding surface temperatures $T_{S,i}$ for $i = 1, \cdots, 6$ can easily be estimated using simple heat transfer equations. Now, six local heat transfer coefficients ($h_{pebble,i}$, for $i = 1, \cdots, 6$) can be calculated, and, finally, the averaged heat transfer coefficients can be obtained by averaging these six coefficients.

$$\dot{Q}_{sphere} = \dot{m} c_p \left(T_{outlet} - T_{inlet} \right) \tag{3.1}$$

$$T_\infty = f(z) = \frac{z}{D} \left(T_{outlet} - T_{inlet} \right) + T_{inlet} \tag{3.2}$$

$$h_{pebble,i} = \frac{\dot{Q}_{convection}}{A \left(T_{S,i} - T_\infty \right)} \text{ for } i = 1, \cdots, 6 \tag{3.3}$$

$$\dot{Q}_{sphere} \approx \dot{Q}_{convection} \tag{3.4}$$

$$h_{pebble,average} = \frac{1}{6} \sum_i h_{pebble,i} \tag{3.5}$$

where $\dot{m}$ is the air mass flow rate, c_p is the specific air heat, D is the wireless pebble diameter, z is the distance from the bottom of the wireless pebble in the airflow direction,

35

A is the surface area where the heat is transferred to the wireless pebble, $\dot{Q}_{sphere}$ is the heat obtained from the flowing air in a facility system, $\dot{Q}_{convection}$ is the heat generated in a wireless pebble to be heat-exchanged by convection, $h_{pebble,i}$ is the heat transfer coefficient at the corresponding outer surface at the ith temperature measurement position, and $h_{pebble,average}$ is the average value of the heat transfer coefficients at the outer surface corresponding to the six temperature measurement positions. Furthermore, T_{inlet}, T_{outlet}, $T_{S,i}$, and T_{∞} are the temperatures at the inlet and outlet, the outer surface temperature corresponding to the ith measured inner surface temperature, and the bulk temperature of flowing air, respectively.

3.1.1 Four Nusselt number correlations for comparing heat transfer coefficients

The four different Nusselt number correlations from [3]–[5] were taken and summarized in Table 3.1 to compare the heat transfer coefficients. The Whitaker model [3] was first selected for the forced convection flow empirical equations for heated spheres. Second, assuming that the sphere in the cylindrical tube is a two-concenter cylindrical tube at sphere height, the hydraulic diameter can be set in the modified laminar internal flow model. Third, Yuge [4] conducted heat transfer experiments for forced convection of airflow. Fourth, Kramers [5] performed a steady experiment on airflow with a relatively small Reynolds number on a sphere approximately 1 mm in diameter. In section 3.2, the performance of the wireless pebble is verified step by step through the comparison between the heat transfer coefficient of the wireless pebble surface and the heat transfer coefficient derived from these four Nusselt numerical correlations.

36

Table 3.1 Nusselt number correlations of Whitaker's model [3], the model of modified laminar internal flow, Yuge's model [4], and Kramers's model [5]

Authors	Medium	Nusselt number Correlation	Applicability
Whitaker's model [15]	Air	$Nu = 2 + 0.4\text{Re}^{0.5} + 0.06\text{Re}^{\frac{2}{3}}\text{Pr}^{0.5}\left(\dfrac{\mu_\infty}{\mu_w}\right)^{0.25}$	$0.71 \le \text{Pr} \le 380$ $3.5 \le Re_\text{D} \le 7.6104$ $1.0 \le \mu_\infty/\mu_w \le 3.2$
Model of modified laminar internal flow	Air	$Nu = 4.36$	-
Yuge's model [2]	Air	$Nu = 2 + 0.493\,\text{Re}^{0.5}$	$10 < \text{Re} < 1000$ $\text{Pr} = 0.715$
Kramers's model [16]	Air	$Nu = 0.42\,\text{Pr}^{0.2} + 0.57\,\text{Pr}^{0.31}\,\text{Re}^{0.5}$	$0.4 < \text{Re} < 2100$ $0.71 < \text{Pr} < 380$

3.1.2 Two configurations for TC attachment positions

To further analyze how the location of the TCs affects the result, it is necessary to differentiate the configuration of the TC attachment locations on the inside surface of the wireless pebble. In the first symmetrical TC configuration, as shown in Figure 3.2 (a), the upper plane, in which TC #1 to TC #4 are placed on the four vertices, and the lower plane, in which TC #5 to TC #6 are placed on the diagonals, are the same parallel distance from the center of a cross-section (upper and lower, respectively) of the wireless pebble.

The second asymmetric TC configuration in Figure 3.2 (b), on the other hand, consists of placement in the top (TC #1) and bottom (TC #6) of the sphere, and the front (TC #3) and the left (TC #2) in its center cross-section, and two TCs (TC #4 and TC #5) on the upper and lower planes as defined in configuration (a), respectively.

38
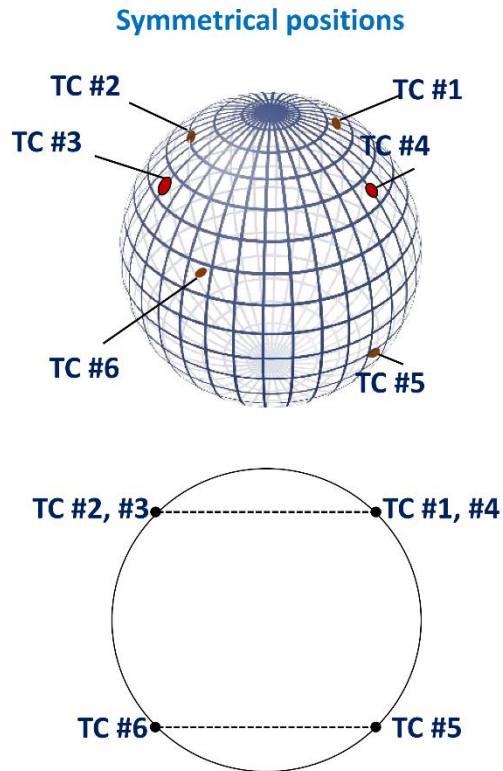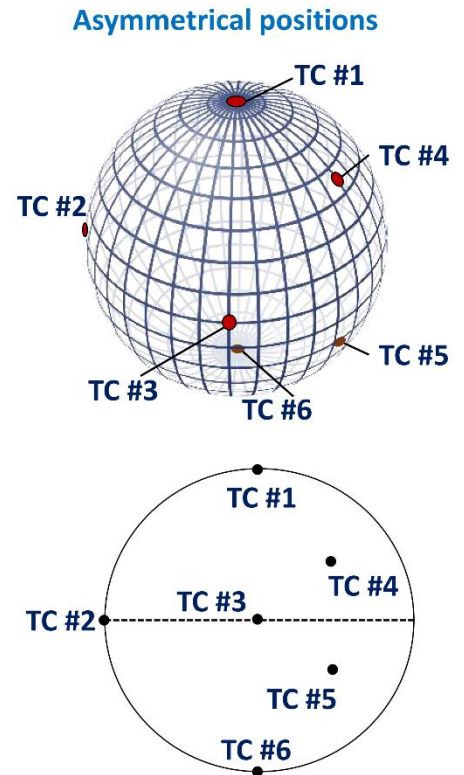
Figure 3.2 Two different TC attachment configurations. (a) Symmetrical: upper plane (TC #1 to TC #4) and lower plane (TC #5 and TC # 6) (b) Asymmetrical: top (TC # 1), bottom (TC # 6), front (TC #3), left (TC #2), and TC #4 and TC #5 on the upper and lower planes as defined in configuration (a), respectively.

3.2 Wireless measurements with change in volume flow rate

In this section, the author first investigates how well the device can measure temperature. The airflow facility described in the previous section was used in measuring the wireless pebble's six internal surface temperatures (TC #1–TC #6) and the inlet and outlet temperatures under varying airflow rates. The first symmetric TC configuration was adopted here. Three different volume flow rates were used: low (12 standard cubic feet per hour (SCFH)), medium (15 SCFH), and high (18 SCFH). Figure 3.3 (a)–(c) shows six temperatures, and inlet and outlet temperatures, and Figure 3.3 (d)–(f) shows the heat transfer coefficients obtained from the steady state temperature information compared with the four Nusselt number correlations described in Section 3.1.

3.3 Effect of locations of TCs

Two similar airflow experiments were conducted to evaluate the effect of TC locations, as in Section 3.2, using two different single wireless pebbles, one with a symmetrical TC configuration and the other with an asymmetrical TC configuration. The flow rate increased from Figure 3.4(a) to (c) from 12 SCFH to 18 SCFH but the three average values $h_{pebble,average}$ from Figure 3.4(d) to (f) were almost identical. As a result, the author concluded that there was no significant difference between the values from the literature and experiments depending on where the TC was attached.

40
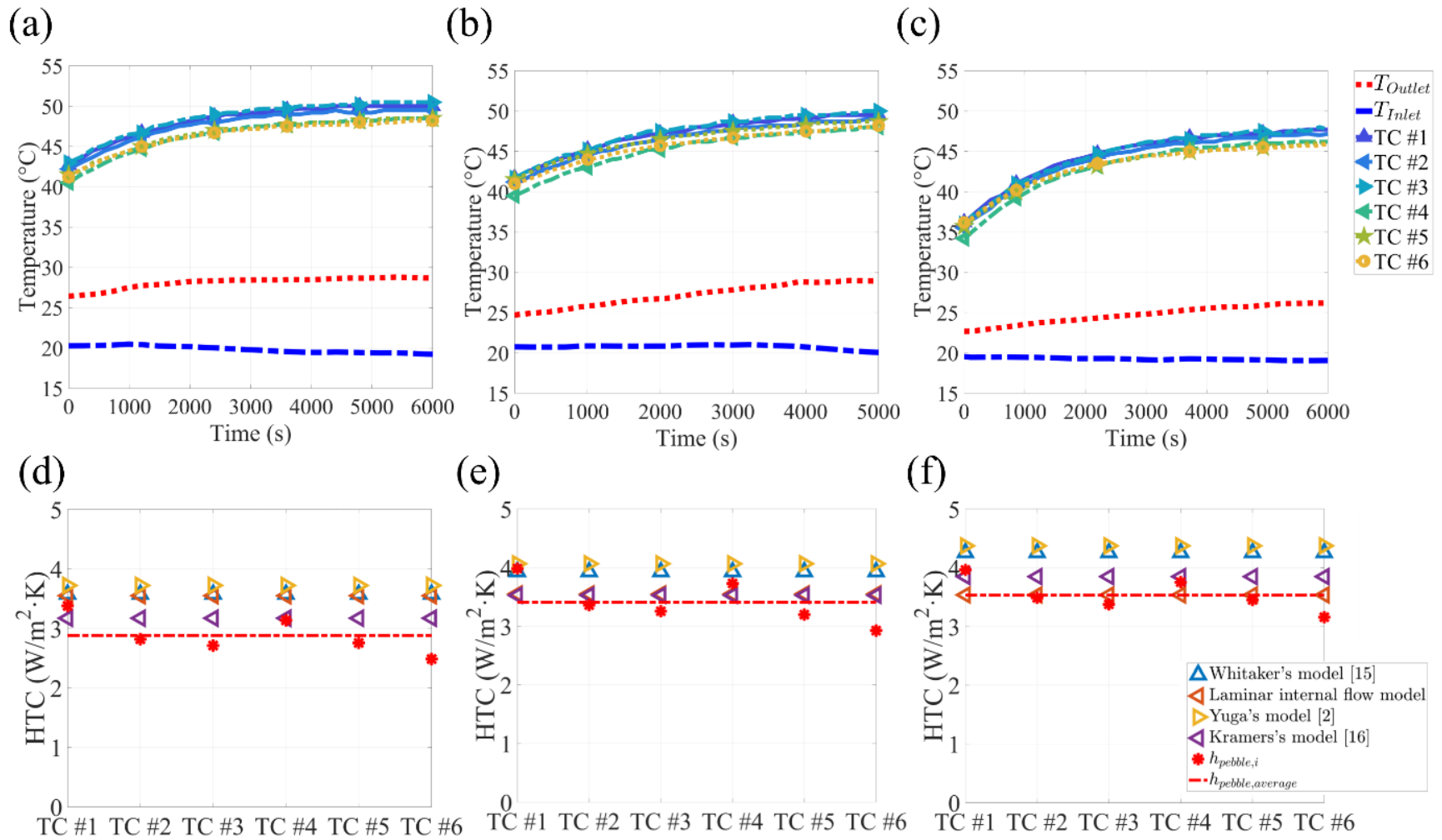
Figure 3.3 Eight temperature profiles (TC #1–TC #6, and inlet, outlet) and comparison of heat transfer coefficients at low (12 SCFH, (a) and (d)), medium (15 SCFH, (b) and (e)), and high (18 SCFH, (c) and (f)) flow rates
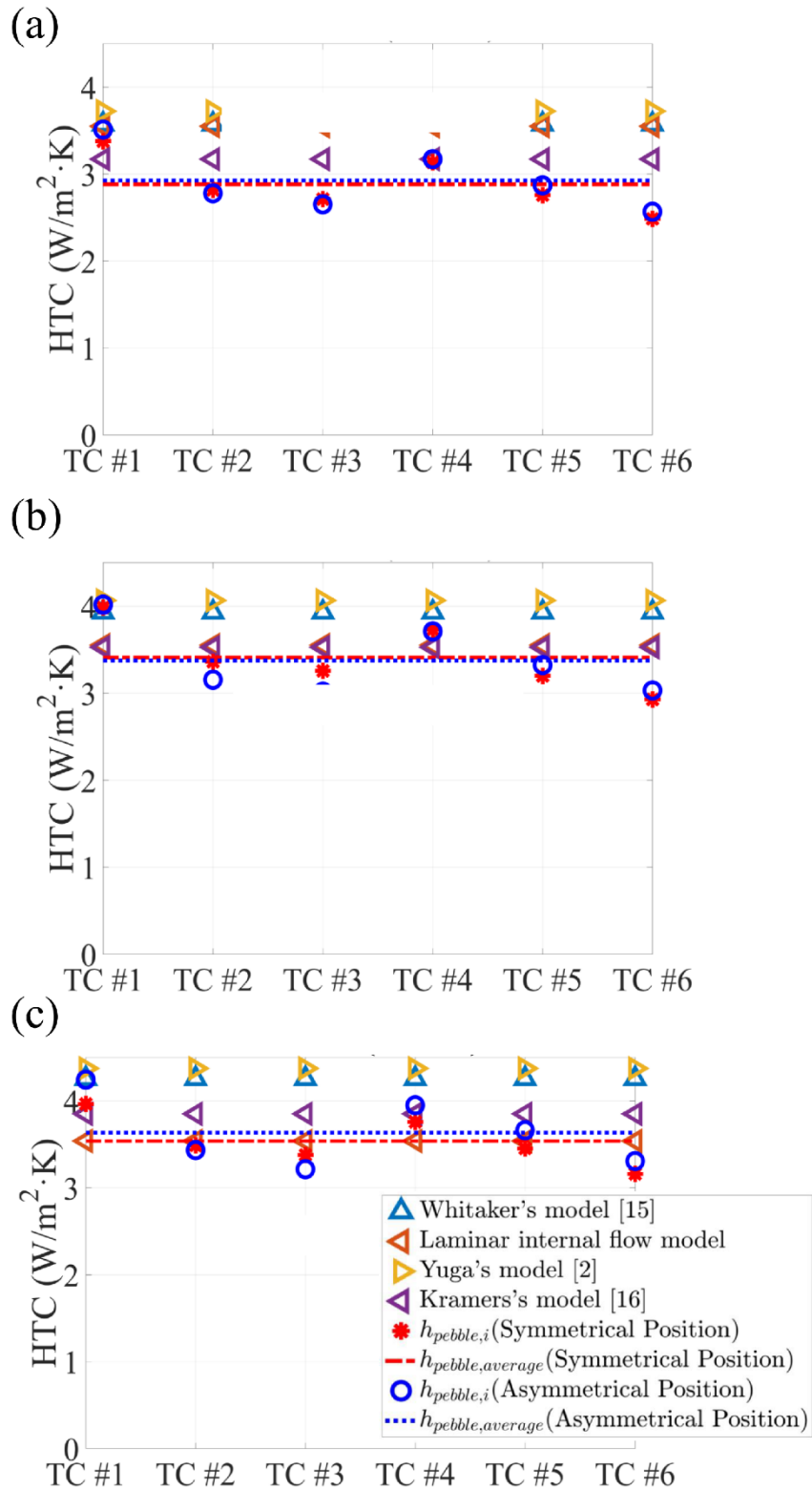
Figure 3.4 Comparison of local heat transfer coefficients (HTC) and averaged heat transfer coefficient obtained from experiments and four correlation models at (a) low (12 SCFH), (b) medium (15 SCFH), and (c) high (18 SCFH) flow rates

3.4 Effect of internal heater orientation

The author examination of the effect of the internal heater orientation is presented in this section. Three different experiments were conducted to differentiate the random three-dimensional orientation of a single wireless pebble, whereas the local h value, $h_{pebble,i}$, and the average h value, $h_{pebble,average}$, were obtained on the basis of steady state temperature information. Table 3.2 shows a statistical analysis of the mean heat transfer coefficient (M, $h_{pebble,average}$) ± standard deviation (SD) and minimum (in the column Min) and maximum (in the column Max) values of each experiment's six heat transfer coefficients ($h_{pebble,i}$ for $i = 1, \cdots, 6$) relative to the heat transfer coefficient derived from the four correlation models referred to in Section 3.1. There was no significant difference in the error range in the average calculation of $h_{pebble,average}$ depending on where the internal heater was placed. This means that it is possible to extend from one pebble to several pebbles, as there was no significant difference in the calculation if multiple wireless pebbles were randomly placed.

Table 3.2 Comparison of averaged heat transfer coefficient $h_{pebble,average}$ obtained from experiments, and four correlation models

Internal Heater Orientation Experiments					Four Correlation Models			
Random Orientation	**N**	**M±SD**	**Min**	**Max**	Whitaker [15]	Laminar internal flow	Yuge [2]	Kramers [16]
#1	6	2.96±0.56	2.20	3.63				
#2	6	3.34±0.41	2.77	3.94	3.93	3.55	4.07	3.53
#3	6	2.76±0.54	2.01	3.36				

43

3.5 Demonstration of multiple wireless pebbles

Finally, an experiment with three identical symmetrical TC configurations was performed on several wireless pebbles. In this case, three wireless pebbles were placed in the same experimental facility, and heat transfer experiments were performed until a stable state was reached. Figure 3.5 shows the configuration of the three wireless pebbles. Each pebble has a different ID; that is, the pebble with ID= 3 is at the bottom, ID= 4 is at the center, and ID= 5 is at the top. The geometric arrangement revealed that the bulk temperature at the bottom of ID=5 was slightly lower than the bulk temperature at the bottom of ID=4, which means that the local bulk temperature depended on the location of the pebble.

Table 3.3 shows a statistical analysis of the mean heat transfer coefficient (M, $h_{pebble,average}$) ± SD and minimum and maximum values of six heat transfer coefficients $h_{pebble,i}$ for $i = 1,\cdots,6$ per experiment compared with the heat transfer coefficient derived from the four correlation models. As can be seen from the results, the values of the averaged $h_{pebble,average}$ of pebbles of ID=5 and ID=3 were considerably different, even though the bulk temperature distribution was considered.

The result shows the average values $h_{pebble,average}$ of the ID=5 and ID=3 pebbles were significantly different, although the bulk temperature distribution was considered. In other words, there were evidently differences in the average heat transfer coefficients $h_{pebble,average}$ between the pebbles, which implies that the average heat transfer coefficients of locally positioned pebbles can differ significantly when extended to the packed pebble-bed system.

44

Table 3.3 Comparison of averaged heat transfer coefficient $h_{pebble,average}$ **obtained from experiments and four correlation models using multiple wireless pebbles**

Multiple Wireless Pebble Experiment					Four Correlation Models			
Pebble (ID, location)	N	M±SD	Min	Max	Whitaker [15]	Laminar internal flow	Yuge [2]	Kramers [16]
3, Bottom	6	3.79±0.24	3.52	4.19	3.93	3.55	4.07	3.53
4, Middle	6	3.09±0.49	2.45	3.76				
5, Top	6	2.96±0.44	2.35	3.60				
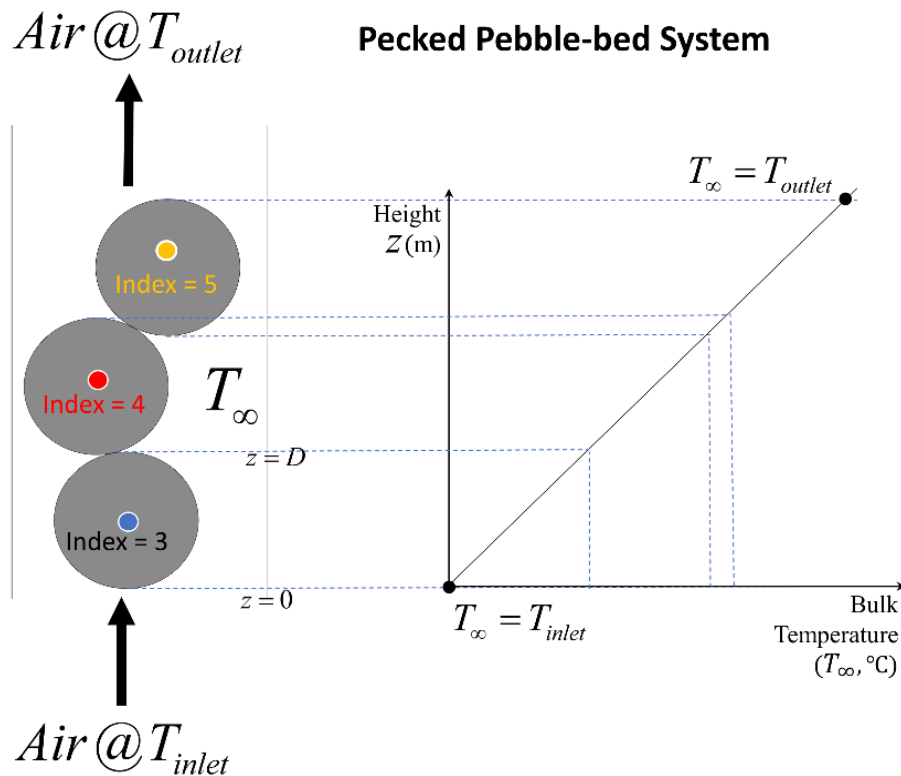
Figure 3.5 Experimental setup of multiple wireless pebble experiments. Three different pebble ID numbers (index numbers) were set to identify the different pebbles. In the heat transfer experiment of the packed bed system, the pebbles with ID=3, ID=4 and ID=5 were placed at the bottom, middle, and top, respectively. Each bulk temperature measurement near the target surface temperature depended on the corresponding geometric location.

4. Analysis of a PWR fuel pin during unprotected LOFA

Suppose that nominal PWR steady-state nuclear fuel is perturbed with a sudden change of inlet mass flow rate to simulate unprotected LOFA transience. The author conducted a simulation of a PWR nuclear fuel pin with *MARS* code [28]. Table 4.1 and 4.2 summarize the detailed fuel geometry and thermal hydraulic parameters, respectively. The fuel rod's axial heating power profile is approximated by a cosine function of the average linear heat generation of 17.86 kW/m.

Table 4.1 Geometry parameters for the reference PWR fuel pin

Heated fuel height	3.88 m
Rod-to-rod pitch	12.60 mm
Fuel rod outside diameter	9.50 mm
Fuel pellet diameter	8.19 mm
Cladding inner diameter	4.18 mm
Cladding thickness	11.78 mm
Gap diameter	0.57 mm

Table 4.2 Operational parameters for PWR pin simulation

Inlet temperature	293.10 ℃
Operational pressure	15.51 MPa
Pin-average linear heat generation	17.86 kW/m
Peak linear heat generation	28.05 kW/m
Steady-state mass flux	3675.40 kg/m2·s
Inlet temperature	293.10 ℃
Operational pressure	15.51 MPa

46

A total of 97 independent *MARS* simulation cases were created to simulate an unprotected LOFA by suddenly reducing the flow rate to only 3% of the nominal steady-state flow rate (i.e., 100% → 3%). Transient outlet temperatures and local fuel temperatures for each simulated case were reported for SVM training.

4.1 SVM for LOFA

SVM algorithms have become a widely used as a classification method since the introduction of Cortes and Vapnik (1995). They offer many benefits for the classification of patterns and model regression [30]–[35]. The first SVM algorithm was intended to classify where the new point belongs to. The given data points $\{x_1, \cdots, x_n\}$ belong to two classes $y_i \in \{1, -1\}$, where the class label of point x_i is for $i = 1, \cdots n$. An SVM finds the hyperplane $\boldsymbol{w}$, also called the decision boundary, that best separates the data points in the training set by the class labels $\{1, -1\}$. The governing equation of an SVM is formulated as follows:

$$\text{To minimize } \frac{1}{2}\|\boldsymbol{w}\|^2 = \boldsymbol{w}^T\boldsymbol{w}, \text{ subject to } y_i(\boldsymbol{w}^T x_i + b) \geq 1, \forall i. \tag{4.1}$$

This constrained optimization problem is reorganized into:

$$\text{To minimize } \frac{1}{2}\|\boldsymbol{w}\|^2, \text{ subject to } 1 - y_i(\boldsymbol{w}^T x_i + b) \leq 0, \forall i. \tag{4.2}$$

After the gradient of its Lagrangian multiplier L is set to zero in relation to $\boldsymbol{w}$ and b, the equation becomes:

$$L = \frac{1}{2}\boldsymbol{w}^T\boldsymbol{w} + \sum_{i=1}^{n} \alpha_i \left(1 - y_i(\boldsymbol{w}^T x_i + b)\right) \tag{4.3}$$

$$w = \sum_{i=1}^{n} \alpha_i y_i x_i, \sum_{i=1}^{n} \alpha_i y_i = 0, \alpha_i \geq 0. \tag{4.4}$$

Then the dual optimization form for an SVM is obtained:

47

$$\text{max.}\, W(\alpha) = \sum_{i=1}^{n} \alpha_i - \frac{1}{2}\sum_{i=1,j=1}^{n} \alpha_i\, \alpha_j y_i y_j x_i^{\ T} x_j$$

$$subject\ to\ C \geq \alpha_i \geq 0, \sum_{i=1}^{n} \alpha_i y_i = 0. \quad (4.5)$$

where α_i and α_j are the Lagrangian multipliers, and C is a regularization parameter [36], [37]. This is a convex quadratic programming (QP) problem for which there is always a global maximum of α_i and numerous established solving tools. With the optimal values of α_i and α_j, which can obtain the support vectors, the above QP problem can be obtained efficiently [38].

 Not only can this algorithm linearly separate the mapped data, but it can also be used if the mapping function is not known explicitly, and its inner product can be even calculated. Kernel techniques were first introduced by Vapnik (1992) as the transformation from input data x_i to a higher-dimensional space. The algorithm has also shown that it can make the problem easier to solve. If the original input space, x, is transformed into a higher-dimensional feature space, $\phi(x)$, the kernel function K is obtained as the inner product $K(x_i,x_j) = \phi(x_i) \cdot \phi(x_j)$ of the mapping function. In fact, various kernel features have been introduced, such as the linear kernel in Figure 4.1 (a), the homogeneous polynomial kernel, the Gaussian radial base function (RBF) kernel in Figure 4.1 (b), and the hyperbolic tangent. Using this kernel function, the SVM dual optimization formula becomes:

$$\text{max.}\, W(\alpha) = \sum_{i=1}^{n} \alpha_i - \frac{1}{2}\sum_{i=1,j=1}^{n} \alpha_i\, \alpha_j y_i y_j K(x_j, x_j)\ subject\ to\ C \geq \alpha_i \geq 0, \sum_{i=1}^{n} \alpha_i y_i = 0$$

$$(4.6)$$

(a) Linear Kernel : Transform $\phi(x) = x$

Misclassified point

$Margin$
$m = \dfrac{2}{\|w\|}$

w

Support vector

Class 2

Support vector

$w^T\phi(x) + b = 1$

Class 1

$w^T\phi(x) + b = 0$

$w^T\phi(x) + b = -1$
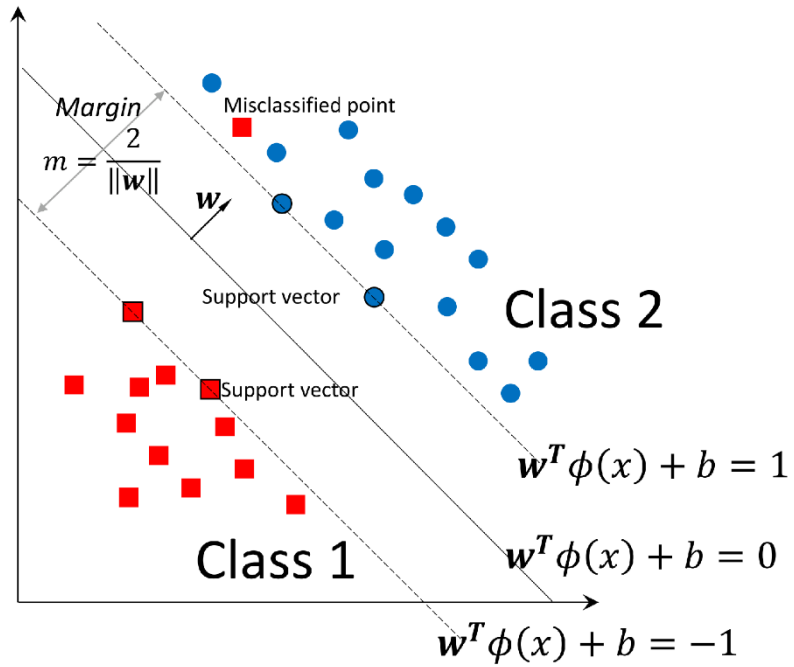
(b) RBF Kernel : $K(x_i, x_j) = \exp\left(\dfrac{-\|x_i - x_j\|^2}{\sigma}\right)$
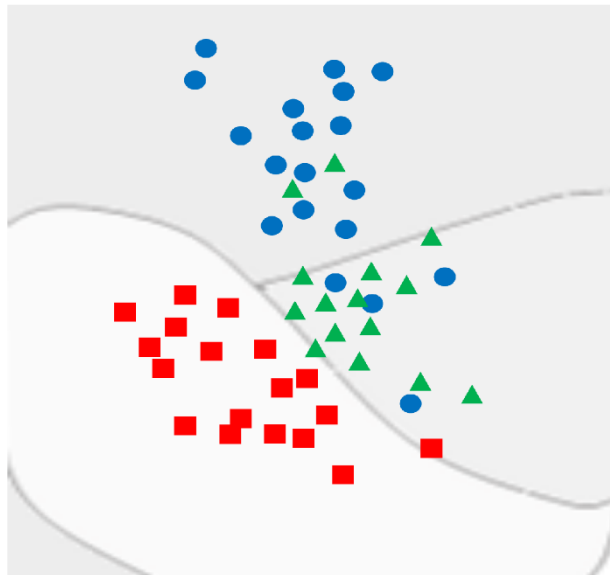
Figure 4.1 SVM with kernel function (a) linear kernel (b) Gaussian RBF kernel

Hsu and Lin (2002a and 2002b) initiated comparisons of methods for multi-class vector support machines and compared numerous multi-class SVMs, such as BSM and LIBSVM. How to effectively extend a multi-class SVM is an ongoing problem that is beyond the scope of this study. Here, an error-correcting output code (ECOC) model [42] was used. This algorithm used the $K(K-1)/2$ binary SVM model, and a "one-versus-one" coding design in which K is the number of unique class labels. In an ECOC strategy, a classifier can be created to target classifications between different sub-sets. This means that these subsets can divide the main problem of classification into tasks of sub-classification. The author created an SVM training template with an ECOC model and a Gaussian RBF linear kernel for predictions based on *MARS* simulated results.

4.2 MARS simulation results for a nuclear fuel pin during an unprotected LOFA

A reduced flow rate increases the outlet temperature. Figure 4.2 illustrates the transience of outlet temperature in flow reduction test cases. As soon as flow reduction starts, the outlet temperature tends toward a new equilibrium. The rate at which it achieves equilibrium is determined by the heat transfer rates coupled with continuity, momentum, and energy balance with constitutive equations. In Figure 4.2, mass flow (G) is defined as the mass flow rate divided by flow area, and mass flow ratio (G ratio) is defined as the mass flow rate ratio after and before the occurrence. Because the flow area is the same before and after the events, the G ratio reflects how G changes.
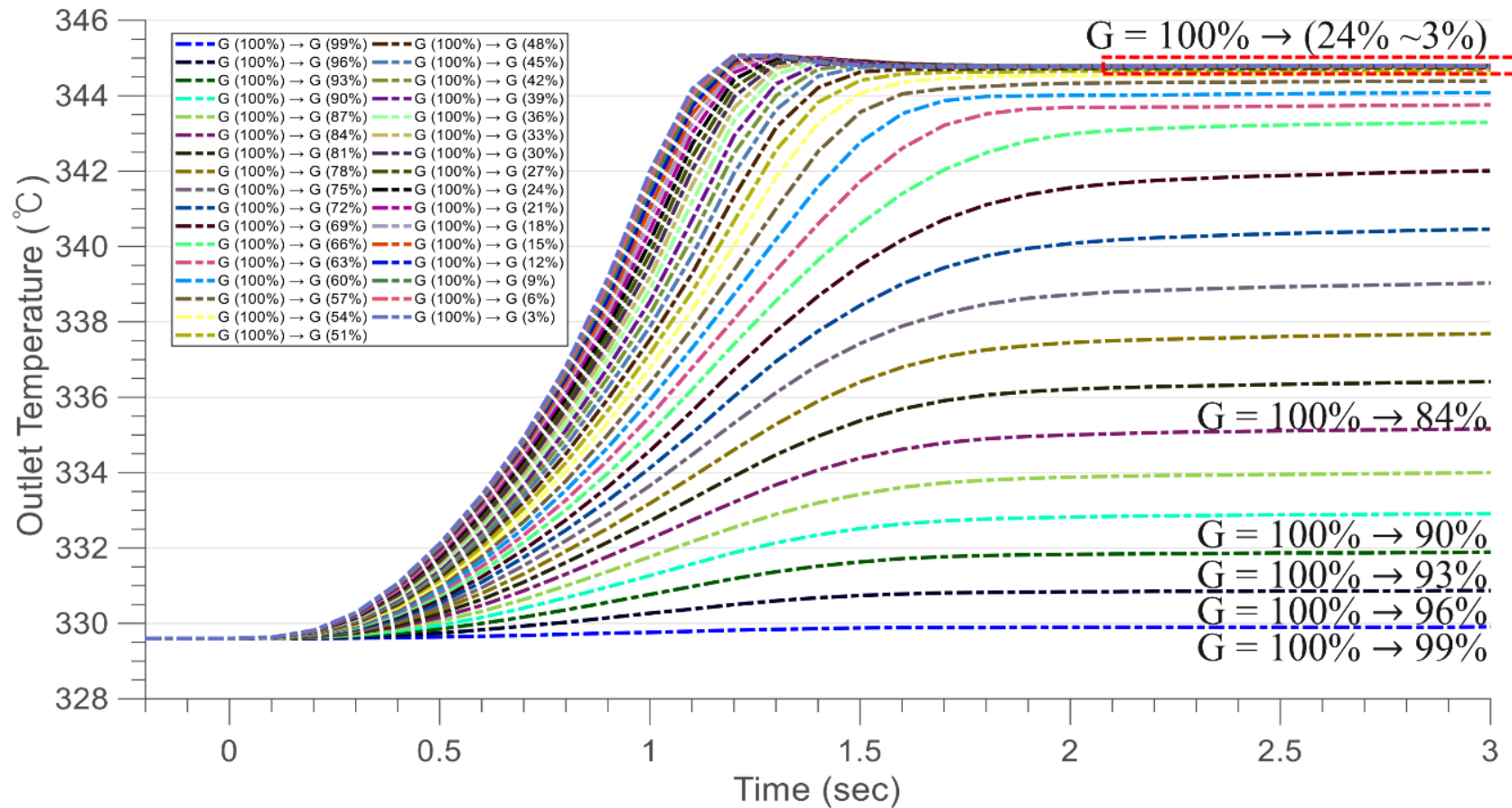
Figure 4.2 Overall outlet temperature profiles as the mass flow ratio decreases. Each line represents a reduction in mass flow rate by more than 3% compared to the next-lower line

As the outlet flow temperature escalates, the fuel surface undergoes a change in heat transfer mode due to overheating. Figure 4.3 (a), (b), and (c) show different flow regimes along the height of the fuel rod under LOFA due to different flow reductions. An increasing drop in flow rate eventually causes an appreciable two-phase heat transfer, characterized by a nucleate, transition, and film (post-CHF) boiling regime. The higher bulk fluid temperature toward the end of the flow channel, in conjunction with the cosine power profile, leads to the onset of film boiling (at the occurrence of CHF) in the upper half of the fuel rod.

The changes in heat transfer rates result from changes in heat transfer modes. Figure 4.3 (d), (e), and (f) indicate heat transfer coefficients along height of the fuel with respect to LOFA duration. If film boiling is generated, heat transfer rates, expressed as heat transfer coefficients, deteriorate.

Such dynamic heat transfer rate evolutions associated with boiling mode changes influence the rate of energy transfer to the bulk fluid, which is highly related to the rate at which the outlet flow temperature finds a new equilibrium, as shown in Figure 4.3. Consequently, the rate of increase of outlet flow temperature T_{out} during a LOFA contains information concerning changes in the dynamic heat transfer rate.

52
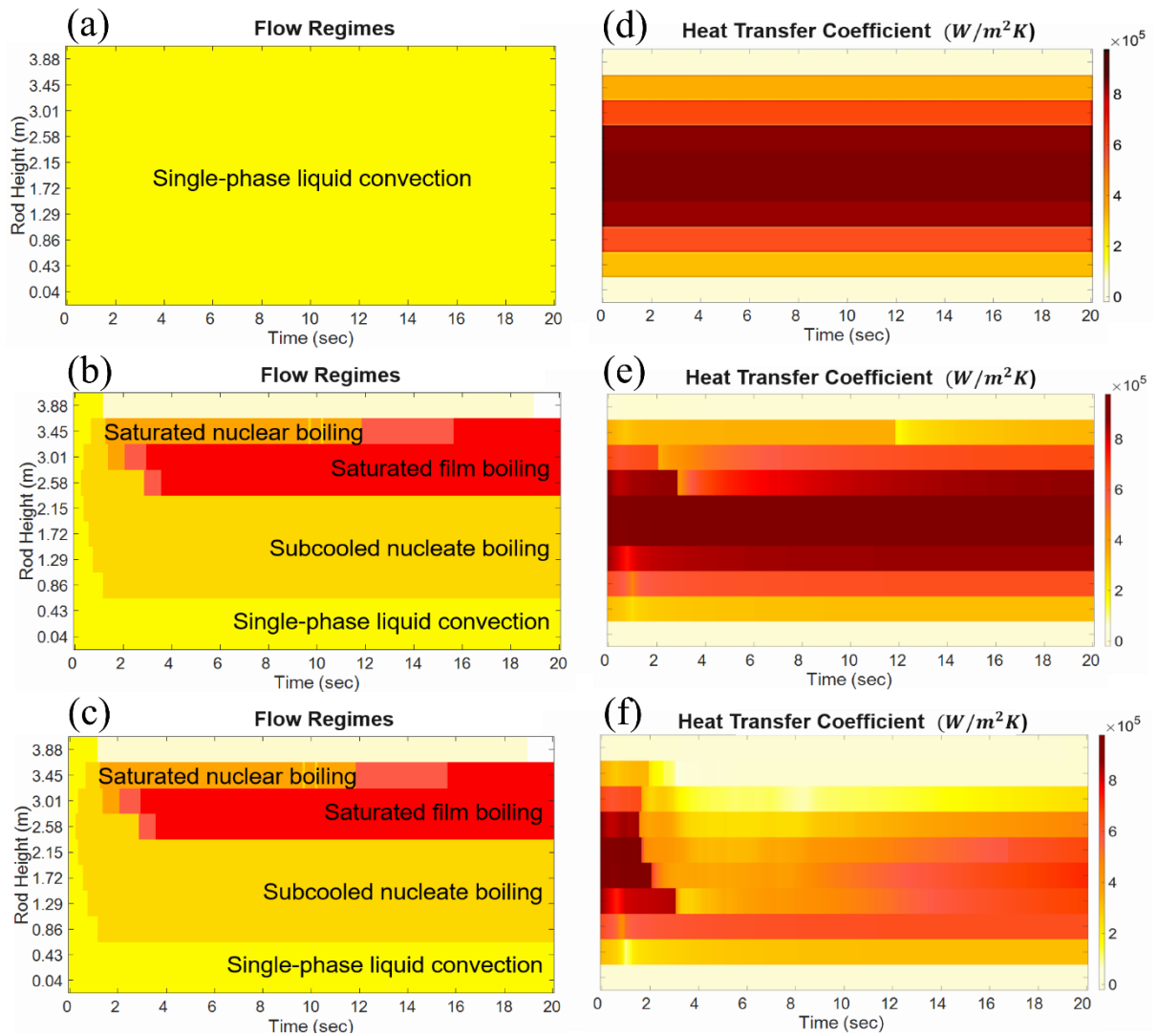
Figure 4.3 Difference in flow regimes and coefficients of heat transfer due to a decrease in the G ratio from G100% to (a),(b) G99 %; (c) and (d) G23%; and (e) and (f) G3%;

The peak fuel and cladding temperatures during LOFA transience are linked to the reduced flow rate. Figure 4.4 represents the peak fuel and cladding temperatures during LOFA transience with respect to the reduced inlet G. The peak temperature is insensitive to flow rate reduction up to the threshold point. However, if the threshold is surpassed, the flow rate decreases. The reduced flow rate at these thresholds is a case in which the flow is sufficiently low to cause the onset of film boiling.

Reducing the flow rate beyond this point will further lower the heat transfer rate, thus increasing the fuel and cladding temperature. The results presented indicate that local peak fuel and cladding temperatures can be predicted by determining the predicted reduced flow at the outlet flow rate. As a result, peak local fuel and cladding temperatures can be predicted using only the measurable outlet flow temperature as input.

The above relationship between different physical quantities during an unprotected LOFA suggests that an inverse operator can be found for accident diagnosis (Figure 1.4). In this study, an SVM trained with *MARS* simulation results is used for finding the inverse operator of the accident diagnosis.

54
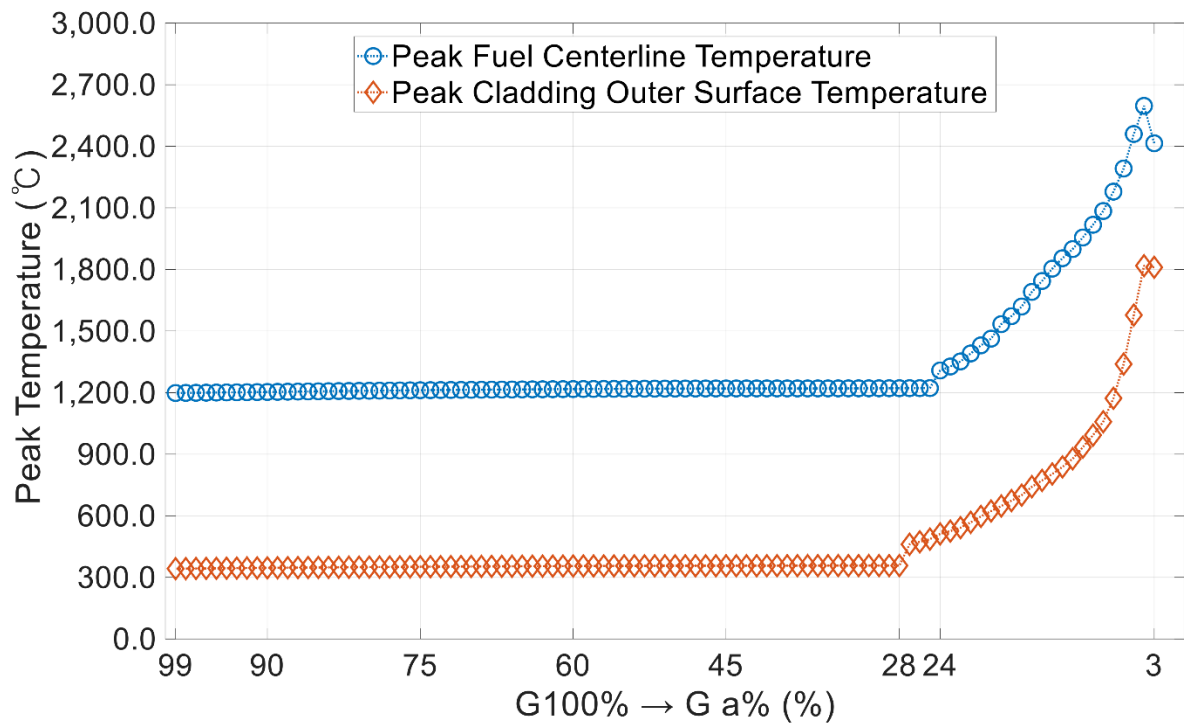
Figure 4.4 Difference in local fuel peak temperatures according to changed inlet mass flux (G) from G100% to G a%

5. Machine learning aided analysis of PWR fuel pin during unprotected LOFA

In the previous section, the author simulated the change in different parameters in accordance with a sudden 97% reduction in mass flow rate via *MARS* simulation. The SVM was then trained with *MARS* results to correlate the following physical quantities:

(1) $T_{out}(t)$ and changed inlet mass flux (G)

(2) $T_{out}(t)$ and peak fuel and cladding temperature

$T_{out}(t)$ is treated as a vector in a time series. Because $T_{out}(t)$ achieved a new equilibrium within 3 s (Figure 4.2), the data in the SVM multi-class input was limited to 3 s of transience. An SVM can divide data into training sets and test sets, as with most machine learning algorithms. The author built an SVM model with training sets and tested it by quantifying the error with a test set for the model. In this study, the author used two metrics to quantify the error, such as mean square error (MSE) and the coefficient of determination (R^2), defined in Eq. (5.1) and (5.2), respectively.

$$R^2(y, y) = 1 - \frac{\sum_{i=1}^{n}\left(y_i - y\right)^2}{\sum_{i=1}^{n}\left(y_i - \bar{y}\right)^2} \tag{5.1}$$

$$MSE(y, y) = \frac{1}{n}\sum_{i=1}^{n}\left(y_i - y\right)^2 \tag{5.2}$$

where n is the number of observations, y_i is the actual value, and $\hat{y}$ and $\bar{y}$ are the prediction and averaged value, respectively. In order to create an SVM model for (1), the parameter G ratio (defined in Section 4) and its corresponding $T_{out}(t)$ became the label and the data for the SVM training data set, respectively. Similarly, for an SVM model for (2), the peak fuel (or cladding temperature) and its corresponding Tout(t) became the label and the data for the SVM training data set, respectively. The effects of the amount if training data and

the transient time of the LOFA on the prediction accuracy are examined for each model. For the sensitivity of the amount of training data, 29 evenly distributed *MARS* simulation results were fixed for the tests, while the number of training data sets was randomly selected and gradually increased from 9 to 68. The transient time of the *MARS* simulation was set to 3.0 s in this case. For this transient time sensitivity of the LOFA, the results of the *MARS* simulation used for SVM training increased gradually from 0.5 to 3.0 s.

5.1 Prediction of the flow rate change $\dot{m}_{in}$ (t) using coolant outlet temperature $T_{out}(t)$

The accuracy of the prediction for flow rate increases with the amount of training data (Figure 5.1). The results show that including 20 percent or more of the training data, or 19 of a total 97 data sets, produces 99 percent accuracy or better for the prediction. In a similar manner, when the training data ratio increased, the MSE approached zero. This implies that there is no need for a large amount of training data to build an SVM relationship between mass flow rate and core outlet temperature.

Figure 5.2 shows the LOFA transient time sensitivity for the prediction accuracy of flow rate change using the core outlet temperature. The prediction accuracy of the flow rate change increased with the increase in LOFA transient time. In the first 0.5 s of LOFA transient time, the prediction accuracy reaches its maximum value for all tested training data ratios. When the amount of training data was less than or near 10% of the entire data set, the saturated accuracy dropped to 0.9 in terms of R^2. This demonstrates that if the training data ratio is higher than 20%, the SVM model trained with the core outlet temperature gives a highly accurate ($R^2 = 0.99$) prediction for the flow rate changes in the first 0.5 s of the LOFA transient time. This suggests that SVM can instantaneously give an accurate prediction of flow rate change upon the occurrence of transience.

57
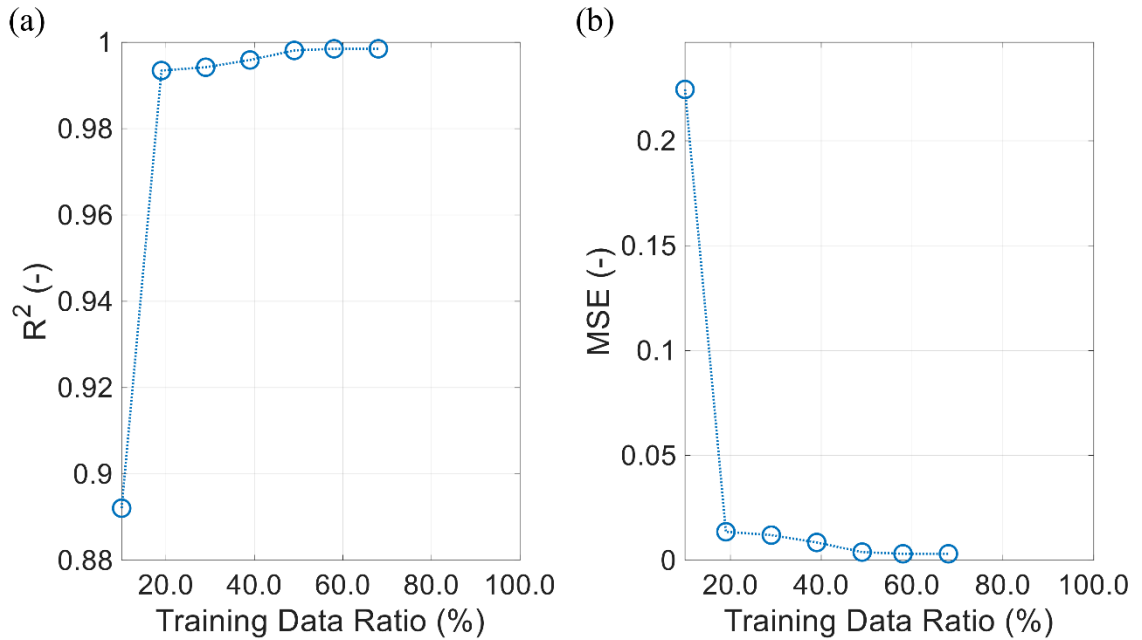
Figure 5.1 Prediction accuracy of flow rate change (G) using core outlet temperature, with respect to the amount of training data. 10% training data ratio represents approximately 9 out of a total 97 data sets. The LOFA transient time is fixed to 3.0 s. (a) R^2, (b) MSE

Figure 5.2 Prediction accuracy of flow rate change (G) using core outlet temperature, with respect to LOFA transient time. 10% training data ratio represents ~9 out of total 97 data sets. (a) R^2, (b) MSE

5.2 Prediction of the peak cladding temperature using coolant outlet temperature $T_{out}(t)$

Furthermore, Figure 5.3 illustrates the predictability (R^2 and MSE) of peak fuel and cladding temperature using the coolant outlet temperature. In Figure 5.3, it is clearly evident that the SVM model can only provide accurate predictions for cladding and fuel surface temperatures, whereas the fuel centerline temperature is difficult to correlate with the core outlet temperature. This means that the core damage initiated by cladding degradation can be predicted by using the core outlet temperature.

  The effect of LOFA transient time on the predictability of the peak cladding outer surface temperature is investigated as shown in Figure 5.4. After approximately 0.5 s, if the number of training data is sufficient, the prediction provides relatively high accuracy (> 0.8). Here, 9 (10% in training data ratio) is shown to be the minimum number of training data sets, as can be inferred in Figure 5.4. LOFA transient temporal sensitivities explain that the extended transient effects are necessarily more accurate (i.e., 20, 30, and 40% of the training data ratio in Figure 5.4). This implies that in the early stages of the unprotected LOFA, changes in the core outlet temperature contain information that is most relevant to the peak cladding outer surface temperature of the entire transience.
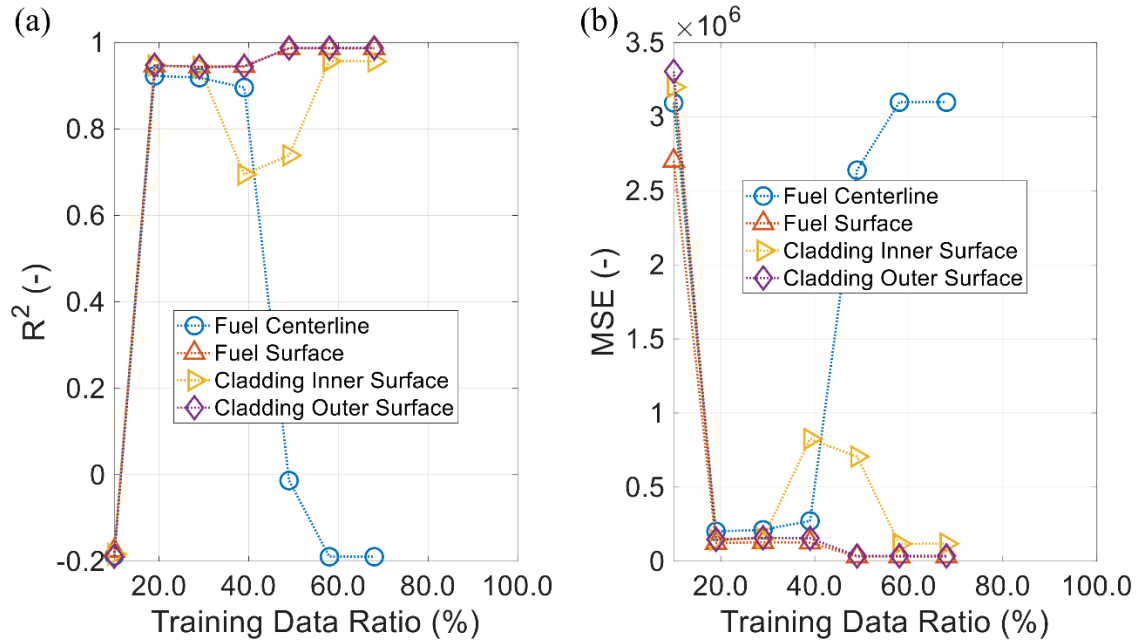
Figure 5.3 Prediction accuracy of peak fuel temperatures using core outlet temperature, with respect to the number of training data. A 10% training data ratio represents approximately 9 data out of total 97 data sets. The LOFA transient time is fixed at 3.0 s. (a) R^2, (b) MSE
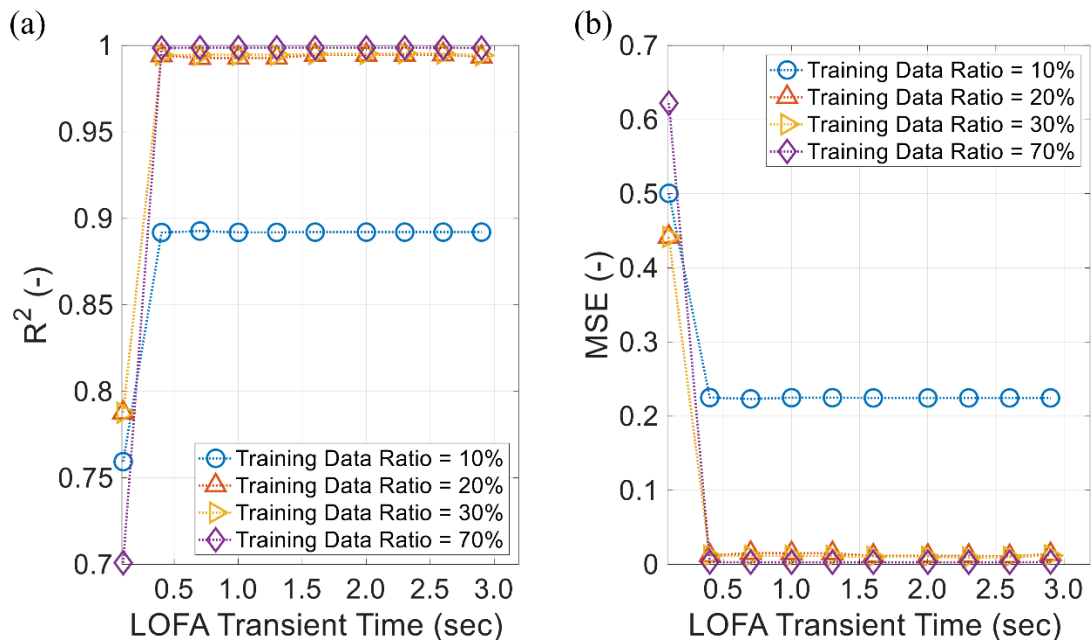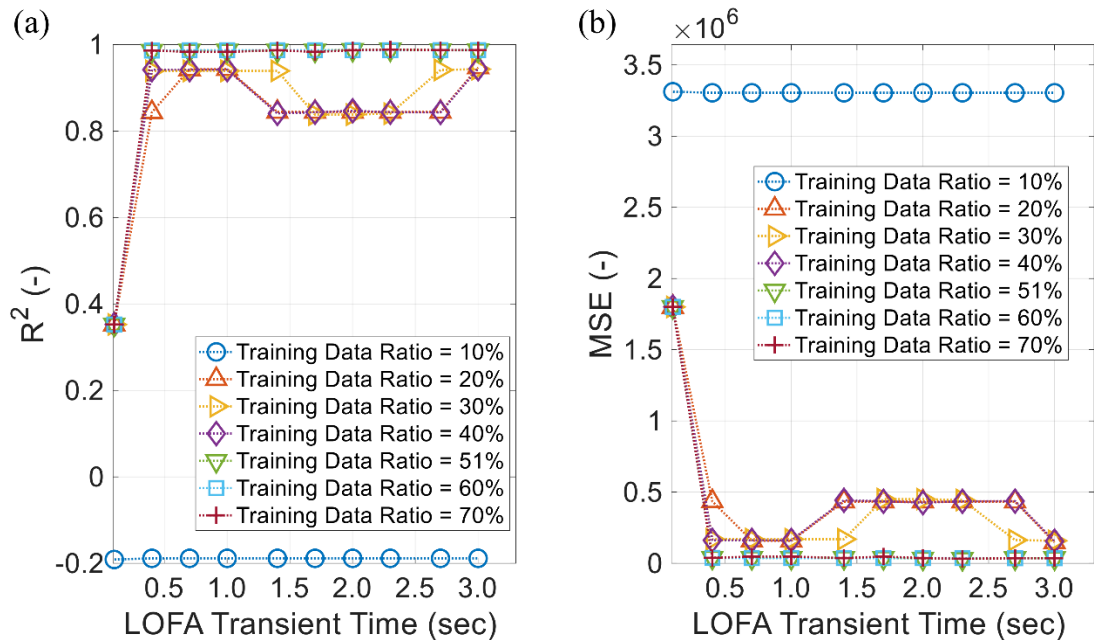

Figure 5.4 Prediction accuracy of peak cladding outer surface temperature using core outlet temperature, with respect to LOFA transient time. 10% training data ratio represents approximately 9 out of total 97 data sets. (a) R^2, (b) MSE

6. Discussions

6.1 Wireless device for heat transfer coefficient of scaled experiments

The author carried out several wireless pebble and simple heat transfer experiments in chapter 3. This study shows in scaled experiments that the local heat transfer coefficient through the implementation of the wireless pebble and simple heat transfer experiments can be quite different. To conclude this, a series of experimental steps were taken.

First, the single wireless pebble did not change the average heat transfer coefficient even when the airflow rate changed and the TC connection structure changed. In addition, because the average coefficient for heat transfer did not change significantly according to the orientation of the internal heater, it could easily be expanded to several wireless pebbles. Lastly, the experiment with three wireless pebbles demonstrated that the wireless pebbles we proposed could greatly help estimate the local heat transfer coefficient.

In particular, this study can be used in the FHR application of an advanced nuclear reactor because the use of Dowtherm A offers practical advantages for conducting scaled experiments.

To design an efficiently scaled experiment for a very large number of packed bed systems, the number of receivers should be increased. There is one principal challenge: as the number increases, the time needed to achieve a stable state can increase, which affects the duration of the battery. This type of problem can be solved by heating the pebbles to increase the initial surface temperatures. This allows the pebbles to reach a stable state quickly, regardless of battery performance.

In summary, the author expects that this study will provide an experimental basis for those who need to measure local temperatures in a non-invasive manner, providing a solid

approach to investigation of non-invasive heat transfer coefficients and randomly packaged configurations in further studies.

In addition, this study not only helps to ensure proper nuclear safety in the future, such as local hot spots due to the random packing of a large number of wireless pebbles, but also serves as a guide to the statistical distribution of local heat transfer coefficients for multiple-pebble systems.

6.2 Implications for SVM-aided LOFA diagnosis

6.2.1 Instantaneous accident diagnosis

It is noteworthy that all the results and analyses presented demonstrate high predictability of flow change and peak fuel temperatures in the early phase of unprotected LOFA (i.e., the first 0.5 s of LOFA transience). This implies that the key accident characteristics are well reflected in the early response to changes in the core parameter (i.e., core outlet temperature). This refers to the possibility of a different intelligent diagnostic framework for accidents than in current practice, depending on the reactor behavior response over prolonged accident progression.

With SVM, however, the early or almost immediate reactor parameters can tell the cause and consequences of unprotected LOFA. This may indicate that SVM-aided accident diagnosis, when combined with current practices, can lead to comprehensive accident diagnoses and reactor safety analyses taking advantage of rich information inherent in accident progression from start to finish. However, the accurate detection of the reactor core's instantaneous response will require advanced core instrumentation technology.

6.2.2 Guidance for accident mitigation strategies

Note that the cases presented are limited to non-protected LOFA. The proven ability to instantly predict the resulting peak fuel temperature and thus the core damage provide an effective guideline for accident mitigation strategies. In other words, SVM can be used to inform reactor operators of the latent consequences of accidents in the early phase of the accident, which can help them choose strategies for coping with accidents.

6.2.3 Strongly correlated response

It is remarkable that even with a limited number of training data, the presented SVM models can achieve exceptionally high prediction accuracy (i.e., $R^2 > 0.9$). This shows clearly that many parameters of reactor response, including those presented in this study, such as T_{out} vs ΔG, and T_{out} vs $T_{cladding, peak}$, are strongly correlated. By means of such strong correlations, one can have access to information that is not directly measurable, such as the initiation of core damage. Consequently, the traditional boundaries of physical locations and physical quantities in accident response and progression detection can be pushed, allowing interdependent detector systems to be made available.

63

7. Conclusion and Future works

In the first study, the accident analysis and accident diagnosis for a nuclear fuel pin during an unprotected LOFA were investigated. In terms of "Accident analysis," MARS, one of the system codes, was used to simulate the changes in physical parameters according to the change in flow during unprotected LOFA. There were the physical parameters we are interested in: 1) core outlet temperatures, 2) flow regimes, 3) heat transfer coefficients of the coolant, and 4) local fuel peak temperatures. In our case study of an unprotected LOFA, the SVM helped to obtain each inverse operator of accident diagnosis in physical quantities: 1) $T_{out}(t)$ and changed inlet mass flux (G) 2) $T_{out}(t)$ and peak fuel and cladding temperature Along the models made by SVM, we have found that the important results. In terms of "Accident Diagnosis", the strongly correlated parameters were found: even with a limited number of training data, the presented SVM models can achieve exceptionally high prediction accuracy (i.e., $R2 > 0.9$). Also, to predict mass flux (G) given $T_{out}(t)$, the key accident features are well reflected in the early response to changes in the core parameter (i.e., core outlet temperature). Using $T_{out}(t)$, the high predictive accuracy of peak cladding outer surface temperature also means the core damage can provide an effective guideline for accident mitigation strategies.

In my opinion, this result can be expanded to analyze some more complex cases in the future. One example is the Reactivity Insertion Accident (RIA) or Loss of Coolant Accident (LOCA) in the design-basis accident (DBA) condition of the water reactor fuel behavior. In fact, the greatest reason why SVM is used in this paper is that the SVM suggests an optimal solution, but other methods such as the ANN and its extensions can be used when one can look at his extensive research area. In recent years, studies on deep learning and reinforcement learning are actively underway. Therefore, if appropriate

64

insights and algorithms are combined, the calculation and prediction for the accident diagnosis in the early phase may be possible.

In the second study, the wireless pebble was designed and developed. The main idea was originated from that Dowtherm A initiates to make the temperature range of interest below 100 °C. Also, it can be demonstrated that the number of pebbles can be extended into applicable for scaled experiments for FliBe. This result provides an experimental basis for those who need to measure local temperatures in a non-invasive manner. In addition, this result serves as a guide to the statistical distribution of local heat transfer coefficients for multiple pebble systems. Lastly, this result helps us ensure proper nuclear safety, such as local hot spots due to the random packing of a large number of wireless pebbles in the future. In the future work of the second study, it is possible to increase the number of wireless pebbles, but at the same time, it is necessary to stabilize the initial heating method in advance. Although the wireless charger that has been developed so far is installed, it is necessary to examine whether it is charging even when the temperature rises. If the number increases, the time to reach the steady-state will be relatively long. Also, software for the real-time check of communication status should be developed when the number is increased to 100. Theoretically, there will be many trial and error in practice if it is possible. Therefore, the problem of battery and careful attention to communication will be the most important in future research.

65

8. References

[1] J. Yang, J. Wang, S. Bu, M. Zeng, Q. Wang, and A. Nakayama, "Experimental analysis of forced convective heat transfer in novel structured packed beds of particles," *Chem. Eng. Sci.*, vol. 71, pp. 126–137, 2012.

[2] R. O. Scarlat and P. F. Peterson, "The current status of fluoride salt cooled high temperature reactor (FHR) technology and its overlap with HIF target chamber concepts," *Nucl. Instruments Methods Phys. Res. Sect. A Accel. Spectrometers, Detect. Assoc. Equip.*, vol. 733, pp. 57–64, 2014.

[3] S. Whitaker, "Forced convection heat transfer correlations for flow in pipes, past flat plates, single cylinders, single spheres, and for flow in packed beds and tube bundles," *AIChE J.*, vol. 18, no. 2, pp. 361–371, 1972.

[4] T. Yuge, "Experiments on heat transfer from spheres including combined natural and forced convection," *J. Heat Transfer*, vol. 82, no. 3, pp. 214–220, 1960.

[5] H. Kramers, "Heat transfer from spheres to flowing media," *physica*, vol. 12, no. 2–3, pp. 61–80, 1946.

[6] T. D. Eastop and C. Smith, "HEAT-TRANSFER FROM A SPHERE TO AN AIR STREAM AT SUB-CRITICAL REYNOLDS-NUMBERS," *Trans. Inst. Chem. Eng. Chem. Eng.*, vol. 50, no. 1, p. 26, 1972.

[7] N. Zweibaum, Z. Guo, J. C. Kendrick, and P. F. Peterson, "Design of the Compact Integral Effects Test Facility and Validation of Best-Estimate Models for Fluoride Salt–Cooled High-Temperature Reactors," *Nucl. Technol.*, vol. 196, no. 3, 2016.

[8]   Wilson M. and H. Jacobs, "A Numerical Solution of the Heat Transfer from a DenseArray of Spherical Particles," in *ANS Proc. National Heat Transfer Conference*, 1993, vol. 7, pp. 225–233.

[9]   J. B. Will, N. P. Kruyt, and C. H. Venner, "An experimental study of forced convective heat transfer from smooth, solid spheres," *Int. J. Heat Mass Transf.*, vol. 109, pp. 1059–1067, 2017.

[10] N. Wakao and S. Kagei, *Heat and mass transfer in packed beds*, vol. 1. Taylor & Francis, 1982.

[11] G. C. Vliet and G. Leppert, "Forced convection heat transfer from an isothermal sphere to water," *J. Heat Transfer*, vol. 83, no. 2, pp. 163–170, 1961.

[12] W. E. Ranz, W. R. Marshall, and others, "Evaporation from drops," *Chem. Eng. Prog*, vol. 48, no. 3, pp. 141–146, 1952.

[13] J. A. Lewis and W. H. Gauvin, "Motion of particles entrained in a plasma jet," *AIChE J.*, vol. 19, no. 5, pp. 982–990, 1973.

[14] M. Nazari, D. J. Vahid, R. K. Saray, and Y. Mahmoudi, "Experimental investigation of heat transfer and second law analysis in a pebble bed channel with internal heat generation," *Int. J. Heat Mass Transf.*, vol. 114, pp. 688–702, 2017.

[15] L. Huddar, J. C. Kendrick, C. Poresky, X. Wang, and P. F. Peterson, "Application of frequency response methods in separate and integral effects tests for molten salt cooled and fueled reactors," *Nucl. Eng. Des.*, vol. 329, pp. 3–11, 2018.

[16] R. S. Abdulmohsin and M. H. Al-Dahhan, "Characteristics of convective heat transport in a packed pebble-bed reactor," *Nucl. Eng. Des.*, vol. 284, pp. 143–152, 2015.

[17] M. V. de Oliveira and J. C. S. de Almeida, "Application of artificial intelligence techniques in modeling and control of a nuclear power plant pressurizer system," *Prog. Nucl. Energy*, vol. 63, pp. 71–85, 2013.

[18] M. He and Y. Lee, "Application of machine learning for prediction of critical heat flux: Support vector machine for data-driven CHF look-up table construction based on sparingly distributed training data points," *Nucl. Eng. Des.*, vol. 338, pp. 189–198, 2018.

[19] M. G. Na, W. S. Park, and D. H. Lim, "Detection and Diagnostics of Loss of Coolant Accidents Using Support Vector Machines," *IEEE Trans. Nucl. Sci.*, vol. 55, no. 1, pp. 628–636, 2008.

[20] M. G. Fernandez, A. Tokuhiro, K. Welter, and Q. Wu, "Nuclear energy system's behavior and decision making using machine learning," *Nucl. Eng. Des.*, vol. 324, pp. 27–34, 2017.

[21] E. Zio, F. Di Maio, and M. Stasi, "A data-driven approach for predicting failure scenarios in nuclear systems," *Ann. Nucl. Energy*, vol. 37, no. 4, pp. 482–491, 2010.

[22] S. G. Kim, Y. G. No, and P. H. Seong, "Prediction of severe accident occurrence time using support vector machines," *Nucl. Eng. Technol.*, vol. 47, no. 1, pp. 74–84, 2015.

[23] J. Liu, R. Seraoui, V. Vitelli, and E. Zio, "Nuclear power plant components condition monitoring by probabilistic support vector machine," *Ann. Nucl. Energy*, vol. 56, pp. 23–33, 2013.

[24] J. W. Hines, D. J. Wrest, and R. E. Uhrig, "Signal Validation Using an Adaptive Neural Fuzzy Inference System," *Nucl. Technol.*, vol. 119, no. 2, pp. 181–193, 1997.

[25] M. Lokanathan and T. Hibiki, "Flow regime, void fraction and interfacial area transport and characteristics of co-current downward two-phase flow," *Nucl. Eng. Des.*, vol. 307, pp. 39–63, 2016.

[26] M. V. de Oliveira and J. C. S. de Almeida, "Application of artificial intelligence techniques in modeling and control of a nuclear power plant pressurizer system," *Prog. Nucl. Energy*, vol. 63, pp. 71–85, 2013.

[27] M. He and Y. Lee, "Application of machine learning for prediction of critical heat flux: Support vector machine for data-driven CHF look-up table construction based on sparingly distributed training data points," *Nucl. Eng. Des.*, vol. 338, pp. 189–198, 2018.

[28] W. J. Lee, B. D. Chung, J. J. Jeong, K. S. Ha, and M. K. Chung, "Development of multi-dimensional realistic thermal-hydraulic system analysis code, MARS 1.3 and its verification," 1998.

[29] C. Cortes and V. Vapnik, "Support vector machine [J]," *Mach. Learn.*, vol. 20, no. 3, pp. 273–297, 1995.

[30] V. Vapnik, "The support vector method of function estimation," in *Nonlinear Modeling*, Springer, 1998, pp. 55–85.

[31] T. Evgeniou, M. Pontil, and T. Poggio, "Regularization networks and support vector machines," *Adv. Comput. Math.*, vol. 13, no. 1, p. 1, 2000.

[32] G. Guo, S. Z. Li, and K. Chan, "Face recognition by support vector machines," in *Automatic Face and Gesture Recognition, 2000. Proceedings. Fourth IEEE International Conference on*, 2000, pp. 196–201.

[33] T. S. Furey, N. Cristianini, N. Duffy, D. W. Bednarski, M. Schummer, and D. Haussler, "Support vector machine classification and validation of cancer tissue samples using microarray expression data," *Bioinformatics*, vol. 16, no. 10, pp. 906–914, 2000.

[34] M. P. S. Brown *et al.*, "Knowledge-based analysis of microarray gene expression data by using support vector machines," *Proc. Natl. Acad. Sci.*, vol. 97, no. 1, pp. 262–267, 2000.

[35] E. Tuba and N. Bacanin, "An algorithm for handwritten digit recognition using projection histograms and SVM classifier," in *Telecommunications Forum Telfor (TELFOR), 2015 23rd*, 2015, pp. 464–467.

[36] A. J. Smola and B. Schölkopf, "A tutorial on support vector regression," *Stat. Comput.*, vol. 14, no. 3, pp. 199–222, 2004.

[37] S. R. Gunn and others, "Support vector machines for classification and regression," *ISIS Tech. Rep.*, vol. 14, no. 1, pp. 5–16, 1998.

[38] H. Drucker, C. J. C. Burges, L. Kaufman, A. J. Smola, and V. Vapnik, "Support vector regression machines," in *Advances in neural information processing systems*, 1997, pp. 155–161.

[39] V. Vapnik, "Principles of risk minimization for learning theory," in *Advances in neural information processing systems*, 1992, pp. 831–838.

[40] C.-W. Hsu and C.-J. Lin, "A simple decomposition method for support vector machines," *Mach. Learn.*, vol. 46, no. 1–3, pp. 291–314, 2002.

[41] C.-W. Hsu and C.-J. Lin, "A comparison of methods for multiclass support vector machines," *IEEE Trans. Neural Networks*, vol. 13, no. 2, pp. 415–425, 2002.

[42] S. Escalera, O. Pujol, and P. Radeva, "On the decoding process in ternary error-correcting output codes," *IEEE Trans. Pattern Anal. Mach. Intell.*, vol. 32, no. 1, pp. 120–134, 2010.

Appendix A: Commercial products selected

[1]   nRF24L01, Single Chip 2.4GHz Transceiver, manufactured by Nordic Semiconductor.

URL:

https://www.nordicsemi.com/eng/content/download/2730/34105/file/nRF24L01_Product_Specification_v2_0.pdf

[2]   Thermocouple breakout board of MAX31855, manufactured by Sparkfun.

URL: https://cdn.sparkfun.com/datasheets/Sensors/Temp/MAX31855K.pdf

[3]   MMC yarn and 'Ultra Heating Fabric', manufactured by Wirekinetics Co., Ltd.

URL :https://www.wirekinetics.com/web/award/upload/files/Fundamental%20of%20Heating.pdf

[4]   ATmega 328/P, manufactured by Microchip Technology Inc.

URL: http://ww1.microchip.com/downloads/en/DeviceDoc/Atmel-42735-8-bit-AVR-Microcontroller-ATmega328-328P_Datasheet.pdf

[5]   5TC-GG-K-30-36, thermocouples manufactured by OMEGA Engineering Inc.

URL :https://www.omega.com/pptst/5TC.html

Appendix B: List of Publications Related to Work

[1]   **Dongjune Chang,** Youho Lee, "Development and validation of wireless pebbles for pebble-bed temperature measurement: non-invasive heat transfer coefficient measurements of flowing air over a sphere", *International Journal of Heat and Mass Transfer* *(under review)*

[2]   **Dongjune Chang,** Maolong Liu, Youho Lee, "Accident Diagnosis of a PWR Fuel Pin during Unprotected Loss of Flow Accident with Support Vector Machine", *Nuclear Engineering Design* *(under review)*

[3]   **Dongjune Chang**, Maolong Liu, Youho Lee, "Analysis of Transient flow change Aided by a Support Vector Machine method", *Nuclear Technology*, March. 2019 *(in preparation)*

[4]   **Dongjune Chang**, Youho Lee, "Preliminary experiments of Wireless Advanced Instrumentation toward Packed Pebble Heat Transfer", *Embedded Topical Meeting On Advances in Thermal Hydraulics, Ath 2018, Held At the American Nuclear Society 2018 Annual Meeting.* Nov. 2018

[5]   **Dongjune Chang**, Maolong Liu, Youho Lee, "Analysis of Transient flow change Aided by a Support Vector Machine method", *Embedded Topical Meeting On Advances in Thermal Hydraulics, Ath 2018, Held At the American Nuclear Society 2018 Annual Meeting.* Nov. 2018 (Recommended for submission to a future special issue of Nuclear Technology for peer-reviewed publication from *American Nuclear Society*)